BACHELOR

Global plasma model for a pulsed helium RF atmospheric pressure plasma jet

van den Biggelaar, Thomas

Award date:
2019

Bachelor Final Project

Global Plasma Model for a pulsed helium RF atmospheric pressure plasma jet

Thomas van den Biggelaar

Supervised by:
ir. T.J.A. (Tim) Staps - EPG, AP, TU/e
ir. B. (Bart) Platier - EPG, AP, TU/e
dr.ir. J. (Job) Beckers - EPG, AP, TU/e

In collaboration with:
dr.ir. J.F.J. (Jesper) Janssen - PlasmaMatters
dr. D.B. (Diana) Mihailova - PlasmaMatters

Eindhoven
July 13, 2019

Contents

Abstract

Atmospheric pressure plasma jets (APPJs) have found to be useful for several surface treatment applications. The corresponding chemistry of these plasmas is of great importance. However, a full understanding of this chemistry is lacking. Experimental methods have been developed in order to determine species densities resulting from these plasmas. Simulations can be used to study the underlying chemistry that results in a certain species density under given conditions and are compared to these experiments. These simulations are made by models that are mostly tailored for certain plasma conditions. As a consequence, there is no general model that can be used for a pure helium APPJ. In this work, a Global Plasma Model (GPM) has been made for the case of a pulsed pure helium RF APPJ with the use of PLASIMO software. It is able to calculate time-evolving volume averaged species densities, electron temperatures and reaction rates. The model is simplified by considering a limited amount of species. It contains a complete set of helium chemical reactions of these considered species, which are applicable to the situation that is considered in this work. Simulations from this model are presented and discussed, which show the performance of this model. Furthermore, the model provides a basis for further helium APPJ model development toward a more complete model that can be used for comparisons with results from experimental methods. Recommendations for further development are provided.

1 Introduction

When an energy source is applied to a neutral gas, some of the present particles can be ionized to form a plasma. This plasma can be generated by electric or electromagnetic fields, which is usually called an electric discharge [5]. Plasmas can be made under different conditions, which determine their properties. One such property of a plasma is the pressure of the neutral gas in which the plasma is created. At low pressures, the plasma is sustained in a thermodynamic non-equilibrium state, meaning that the electron temperature is much higher than the heavy particle temperature. Such a plasma is called a non-thermal plasma. A main advantage of the non-thermal property is that the plasma is stable and is able to maintain a low temperature. These conditions are useful for many plasma applications. The applications are all based on their plasma chemistry, since these plasmas generate usable reactive species that can react with surfaces [15, 41]. For low pressures, the use of non-thermal plasmas are limited due to the use of vacuum systems [40, 41]. Therefore, non-thermal plasmas at the atmospheric pressure regime are introduced. However, higher pressures lead to thermal plasmas, which are unstable. Multiple devices have been developed to make non-thermal plasmas at atmosperic pressure.
An example is the use of an atmospheric pressure plasma jet (APPJ), which is illustrated in Figure 1. A plasma is produced in a tube through which a gas flows. This gas is ionized by an oscillating electric field applied to one of the electrodes. The plasma then exits the tube. A main advantage of this setup is that the reactive species are directly ejected on the surface to be treated. Therefore, the APPJ is investigated for industrial applications such as film deposition, surface cleaning and surface coating [5]. Not only industrial, but also applications in medicine are investigated, such as cancer treatment and wound healing [14].

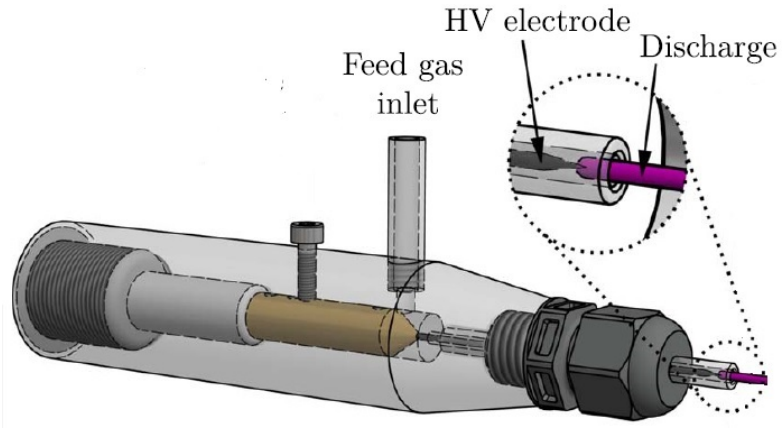

Figure 1: Illustration of an APPJ. The gas flows via an inlet to the electrode, where a discharge is made by the electrodes with an input power. The input power can be generated by a high voltage (HV), for example. The plasma is then ejected from the APPJ on the surface to be treated. Figure from van der Schans et al. [44].

For many of these applications, knowledge of the involved plasma chemistry is of great importance. It will eventually predict which species arrive on the desired surface. Surface treatments by an APPJ are currently based on trial and error, without any knowledge of possible side effects from the plasma. Plasmas have a rich chemistry, which makes it also the biggest challenge in research. Experiments do not provide insight in the detailed mechanisms that lead to plasma properties that are measured by experiments. For example, diagnostics such as Thomson scattering or microwave resonance spectroscopy are used in order to experimentally determine the local or global electron density, respectively [15, 44]. Simulations can be used to study the underlying chemistry that results in a certain electron density under given conditions. Therefore, plasma modeling can help us to understand which species and reactions are dominant. However, these models can be quite complex and are tailored to specific plasma conditions. For this reason, no generally applicable descriptive models exist that are able to be used for a helium plasma APPJ [15].

In this work, a Global Plasma Model (GPM) is developed that is able to model mean value time-dependent species densities produced in an RF pulsed APPJ. This model is also able to model time-dependent electron temperatures and can show which chemical reactions are dominant for the production of a certain species. The APPJ is considered in a pure helium atmosphere. Hence, no impurities are present and pure helium chemistry is the case. The GPM is simplified by considering a limited amount of species. It contains a complete set of the involved chemical reactions of these considered species. These added chemical reactions have been found to be important according to literature. The reactions and present species, with their corresponding properties, are discussed extensively. Simulations have been performed in order to show which results can be obtained from the model. The behavior of this model for certain input parameters is also investigated. Lastly, recommendations for further development are given.
In Section 2, the theory of the balance equations and the helium plasma chemistry is discussed. The description of the model can be found in Section 3. Section 4 provides the results from the simulations and the discussion of these results. Conclusions from the results and discussion are made, which are given in Section 5. Recommendations for further development can be found in Section 6.

2 Theory

In order to model particle densities within a plasma as a result of processes between particles, a 0D-model can be used. In comparison to higher dimensional models, these models only calculate quantities that are averaged over a certain volume. Three main features of plasmas have to be considered when modeling plasma behaviors. One of these features is the configuration, which describes the interaction of the plasma with its environment. Aspects like geometry, boundary conditions and energy coupling are part of the configuration. Transport of species, momentum and energy has also to be taken into account. Species are created and destructed in the plasma and these processes can be described by the plasma chemistry [17]. As mentioned in Section 1, a GPM is used in order to simulate mean values of species and the electron temperature of a pulsed helium plasma jet. Several external control settings can be used like pressure, geometry, input power, the species and the reactions involved during the plasma discharge. The balance equations of the species and energy are described in Section 2.1. The chemical reactions are described in Section 2.2 and their corresponding rate coefficients are elaborated.

2.1 Balance equations

2.1.1 Species balance

The species balance equation can be described by the zeroth moment of the Boltzmann transport equation for species s which is [17]

$$\frac{\partial n_s}{\partial t} + \nabla \cdot (n_s \mathbf{v}_s) = \mathcal{S}_S, \tag{1}$$

where n_s is the density in m^{-3}, $\mathbf{v}_s$ the mean particle velocity in ms^{-1} and $\mathcal{S}_S$ the source term in $m^{-3}s^{-1}$. For simplification, the transport term in the equation can be rewritten by introducing a transport frequency $\mathcal{F}_s$ which is given by

$$\mathcal{F}_s = \frac{1}{n_s} \nabla \cdot (n_s \mathbf{v}_s), \tag{2}$$

the unit of which is s^{-1}. The zeroth moment of the Boltzmann transport equation can then be written as

$$\frac{\partial n_s}{\partial t} + \mathcal{F}_s n_s = \mathcal{S}_s. \tag{3}$$

If the transport term $\mathcal{F}_s$ is only present due to diffusion, it will be given by

$$\mathcal{F}_s = \frac{D_s}{\Lambda^2}, \tag{4}$$

where D_s is the diffusion coefficient for (excited) neutrals in m^2s^{-1} and Λ the characteristic diffusion length in m. Λ is mainly determined by the shortest plasma size [17]. The electric field will play a role for charged particles leading to the addition of a drift component. If quasineutrality is assumed, this extra drift leads to ambipolar diffusion. It is enhanced to [17]

$$D_a = D_s \left(1 + \frac{T_e}{T_h}\right), \tag{5}$$

with T_e the electron temperature and T_h the heavy particle temperature, both in K. The source term S_s depends on the production and destruction mechanisms and it can therefore be split up:

$$\mathcal{S}_s = \mathcal{P}_s - \mathcal{D}_s n_s, \tag{6}$$

where $\mathcal{P}_s$ is the production rate with the same unit as $\mathcal{S}_s$ and $\mathcal{D}_s$ is the destruction frequency in s^{-1}. When more species are considered, the vector notation in the same form as equation (3) is

$$\frac{\partial \mathbf{n}}{\partial t} + \mathcal{F}\mathbf{n} = \mathbf{S}. \tag{7}$$

The production and destruction of particles is due to the chemical reactions that take place. A chemical reaction can simply be visualized by

$$a\mathrm{A} + b\mathrm{B} \longrightarrow c\mathrm{C} + d\mathrm{D}, \tag{8}$$

where a, b, c and d are the stoichiometric coefficients [13]. Equation (8) is an example of the two-body reaction. The general expression for gas or plasma phase reactions is [17]

$$\sum_S v_{s,r}^{\mathrm{d}} X_S \xrightarrow{k_r} \sum_S v_{s,r}^{\mathrm{p}} X_S, \tag{9}$$

in which destruction of species X_S^{d} and production of species X_S^{p} take place. v_s^{d} and v_s^{p} denote the stoichiometric coefficients of destruction and production respectively. k_r is the rate coefficient of the reaction r and can be dependent on the electron temperature T_e of the plasma and the temperature T_g or pressure p of the neutral gas. The reaction rate of reaction r is given by

$$R_r(\mathbf{n}, T_e, T_g, p) = k_r(T_e, T_g, p) \prod_s n_s^{v_{s,r}^{\mathrm{d}}} \tag{10}$$

with unit $\mathrm{m^{-3}s^{-1}}$. Depending on the kind of reaction, the reversed process of a reaction is also possible. The reaction is than visualized by

$$a\mathrm{A} + b\mathrm{B} \longleftrightarrow c\mathrm{C} + d\mathrm{D}, \tag{11}$$

with again the example of a two-body reaction. The reaction rate of the reversed process can be calculated by the use of the principle of detailed balancing:

$$k_{r_1} \prod_s n_s^{v_{s,r_1}^{\mathrm{d}}} = k_{r_2} \prod_i n_i^{v_{s,r_2}^{\mathrm{d}}}, \tag{12}$$

where k_{r_1} is the rate coefficient of the forward reaction and k_{r_2} is the reaction rate of the reversed process. v_{s,r_1} and v_{s,r_2} are the stoichiometric coefficients of destruction. n_s and n_i are the reactants of the reactions for the forward and backward process respectively.
When looking at collisions between electrons and gas species, the rate coefficient can be calculated as follows:

$$k_r = \langle \sigma\left(v_{\mathrm{R}}\right) v_{\mathrm{R}} \rangle_{\mathbf{v}_1, \mathbf{v}_2} = \int \mathrm{d}^3 v_1 \mathrm{d}^3 v_2 f_1\left(\mathbf{v}_1\right) f_2\left(\mathbf{v}_2\right) \sigma\left(v_{\mathrm{R}}\right) v_{\mathrm{R}}, \tag{13}$$

where v_1 and v_2 are the velocities of the colliding species in $\mathrm{ms^{-1}}$, $v_R = |v_2 - v_1|$ the relative velocity in $\mathrm{ms^{-1}}$, σ the collisional cross section in $\mathrm{m^2}$ and f_1 and f_2 the distribution functions of both colliding species normalized to unity [26]. The expression of k_r can be written to an integration over the electron energy space ϵ. It can be assumed that the velocity of electrons is relatively high compared to that of the heavy particles. The function then reads

$$k_r = \int_{\Delta\epsilon_r}^{\infty} \sigma(\epsilon) v(\epsilon) F(\epsilon) \mathrm{d}\epsilon, \tag{14}$$

where $\Delta\epsilon_r$ is the minimal energy needed to let the reaction r take place and v is the electron velocity in $\mathrm{ms^{-1}}$ [23, 26]. In this case, $F(\epsilon)$ is the electron energy distribution function (EEDF). The expression of the rate coefficient can also be written as [18]

$$k_r = \gamma \int_0^{\infty} \varepsilon \sigma(\epsilon) F_0 \mathrm{d}\varepsilon, \tag{15}$$

with F_0 the EEDF, which is proportional to the distribution function of electrons and γ is a constant given by

$$\gamma = \sqrt{\frac{2e}{m_e}}, \tag{16}$$

with e the electron charge and m_e the electron mass.

2.1.2 Energy balance

Plasmas are created by electromagnetic fields, where the net force applied to electrons and ions created by these fields are of similar order of magnitude. Electrons have a much larger velocity than ions since electrons have a much lower mass. If electrons have enough energy, they are able to induce processes like excitation, ionization or dissociation. Because of the high mass difference between ions and electrons, the energy transfer in the collisions between them is inefficient. Therefore, the energy balance equations for the electron temperature T_e and heavy particle temperature T_h, both in K, are separated [23]. The heavy particle temperature is also called the gas temperature T_g, which is also in K. It will be mainly used from Section 2.2 and beyond unless stated otherwise. The energy balance for the electron temperature is

$$\frac{\partial}{\partial t}\left(\frac{3}{2}n_e k_B T_e\right) = P_{\text{input}}(t) - Q_{\text{inelas,e}} - Q_{\text{elas}} + Q_{\text{Ohm}}, \tag{17}$$

where P_{input} is the power input per volume with unit Wm^{-3}. $Q_{\text{inelas,e}}$ is the power per volume dissipated as a result of the energy losses of electrons related to inelastic collisions of electrons. Examples of inelastic collisions are excitation and ionization processes. $Q_{\text{inelas,e}}$ is given by [17]

$$Q_{\text{inelas,e}} = \sum_r E_{e,r} R_r = \mathbf{E}_e \cdot \mathbf{R}, \tag{18}$$

where $\mathbf{E}_e$ is the vector of electron energy transfers per reaction. The total inelastic power loss per volume Q_{inelas} is [23]

$$Q_{\text{inelas}} = Q_{\text{inelas,e}} + Q_{\text{inelas,h}} = \sum_r \Delta h_r R_r, \tag{19}$$

with Δh_r the enthalpy change of the reaction and R_r is given by equation (10). $Q_{\text{inelas,h}}$ is the power per volume from inelastic collisions between heavy particle species. Q_{Ohm} is the power per volume due to Ohmic heating and Q_{elastic} is the power per volume from elastic collisions which is given by [23]

$$Q_{\text{elas,eh}} = \sum_{h \neq e} \frac{3}{2} k_B \left(T_e - T_h\right) 2 \frac{m_e}{m_h} n_e \nu_{eh}, \tag{20}$$

with k_b the Boltzmann constant, m_e the electron mass in kg, m_h the heavy particle mass, n_e the electron density in m^{-3} and ν_{eh} the average collision frequency between the electrons and heavy particle species in s^{-1}. The elastic collisions between electrons and heavy particles lead to an energy transfer from the electrons to the heavy particles. Ohmic heating is generated from the drift of the electrons due to the electric field that is present in the plasma [26]. An expression for ν_{eh} is

$$\nu_{eh} = n_h \sqrt{\frac{8 k_B T_h}{\pi m_{eh}}} \overline{Q}_{eh}, \tag{21}$$

where m_{eh} is the reduced mass from the electron mass and heavy particle mass in kg and $\overline{Q}_{eh}$ is the average momentum cross section in m^2.
Electrons collide with heavy particles elastically or inelastically. So there is an energy transfer from the electrons to the heavy particles. The energy balance for the heavy particles is

$$\frac{\partial}{\partial t} \sum_{i \neq e} \left(\frac{3}{2} n_i k_B T_h\right) = Q_{\text{elas}} + Q_{\text{inelas},e} - Q_{\text{rad}}, \tag{22}$$

with Q_{rad} the power density loss due to radiation of excited heavy and particle species.

2.1.3 Source term and branching ratio

As mentioned before, the total source term consists of a production and destruction term of the species. The total source term can therefore be determined by the use of the net stoichometric

coefficient $W_{S,r}$ of the reaction, which is given by

$$W_{S,r} = v^p_{S,r} - v^d_{S,r}. \tag{23}$$

With the use of equation (23), a mathematical description of the source term $\mathcal{S}_s$ in equation (1) is given by

$$\mathcal{S}_s = \sum_r \left(v^{\mathrm{p}}_{s,r} - v^{\mathrm{d}}_{s,r}\right) R_r = \mathbf{W}_s \cdot \mathbf{R}, \tag{24}$$

where $\mathbf{W}_s$ is a vector of the net stoichiometric coefficients and $\mathbf{R}$ the vector of reaction rates, of which both are one per reaction. Note that the source term calculated from expression (24) is only for one species. The source term must be calculated for every species when a set of species is the case.
A branching ratio BR can be introduced in the case that two or more reactions from the same reactants are possible resulting in different products. This is also introduced for the reverse case where the products remain the same but the reactants may differ. It can be put in equations (13) to (15) outside the integral when assuming that BR is energy independent. If electrons are not involved in the reaction, this BR can just be multiplied by the expression of k_r. The unit of k_r depends on the number of destructed species in equation (9) with its stoichiometric coefficients. This is because of the fact that the unit of the reaction rate remains the same and the number of species in the reaction is variable. For simple 2-body reactions, the unit of rate coefficient is $\mathrm{m^3s^{-1}}$ whereas for simple 3-body reactions the unit is $\mathrm{m^6s^{-1}}$.

2.2 Plasma chemistry

In this section, several chemical reactions which are relevant for helium discharges are discussed. Not all elementary processes and rate coefficients are accurately known. Especially the rate coefficients k_r that are temperature dependent have large ranges of errors or are valid in a narrow range [3], which can result in discrepancies in the model. Some of them are unknown. Therefore, the expressions of the rate coefficients corresponding to the chemical reactions are elaborated. The rate coefficients k_r of the electron involved reactions can also be calculated by equation (15) if the cross sections are available. All units of k_r are $\mathrm{cm^6s^{-1}}$ or $\mathrm{cm^3s^{-1}}$, depending on the reaction as explained in Section 2.1.1.

2.2.1 (Super)elastic collisions, (de-)excitations and quenching

Helium atoms are able to collide with electrons elastically. The elastic collision between a ground state helium atom and an electron is given by

$$\mathrm{He} + \mathrm{e} \longrightarrow \mathrm{He} + \mathrm{e}. \tag{25}$$

If the electron energy is high enough, helium ground state atoms are able to be converted to excited state atoms due to collisions. Moreover, these excited states can again collide with electrons resulting in a higher excited state or de-excitation to a lower excited state. The excitations are mainly inelastic collisions and the de-excitations are mainly superelastic collisions. The general reaction scheme is

$$\mathrm{He}(n,l,s) + \mathrm{e} \longleftrightarrow \mathrm{He}\,(n',l',s') + \mathrm{e}. \tag{26}$$

n is the principle quantum number, l is the total angular momentum and s is the spin of the excited state. The potential energies of the excited and ionized states of helium are illustrated in Figure 2. The energy differences between these states define the electron energy needed for excitation. Only helium excited atoms in the $n = 2$ state are considered in this work, so reactions involving excited atoms with $n > 3$ are not treated.
The rate coefficient that corresponds to such a reaction can be calculated from equation (15) with the corresponding energy dependent cross sections. Also, without using cross sections, an

expression for k_r of the excitation reactions from the ground state to the upper state $n = 2$ is determined by Yuan and Raja [50] and is found to be

$$k_r = 2.308 \times 10^{-10} * BR * T_e^{0.31} \exp\left(-\frac{2.297 \times 10^5}{T_e}\right). \tag{27}$$

The BR takes place in the equation since the reactants can be converted to four possible $n = 2$ excited states, namely He(2^3S), He(2^1S), He(2^3P) and He(2^1P). Yuan and Raja [50] also calculated the rate coefficient of the de-excitation process from $n = 2$ with the use of detailed balancing. It is given by

$$k_r = 1.099 \times 10^{-11} * BR * T_e^{0.31}. \tag{28}$$

A couple of studies have been done to investigate the rate coefficients of the superelastic collisions from one $n = 2$ state to another $n = 2$ state or the ground state. A complete list of them can be found in Belmonte et al. [3], Deloche et al. [9] and Emmert et al. [12].

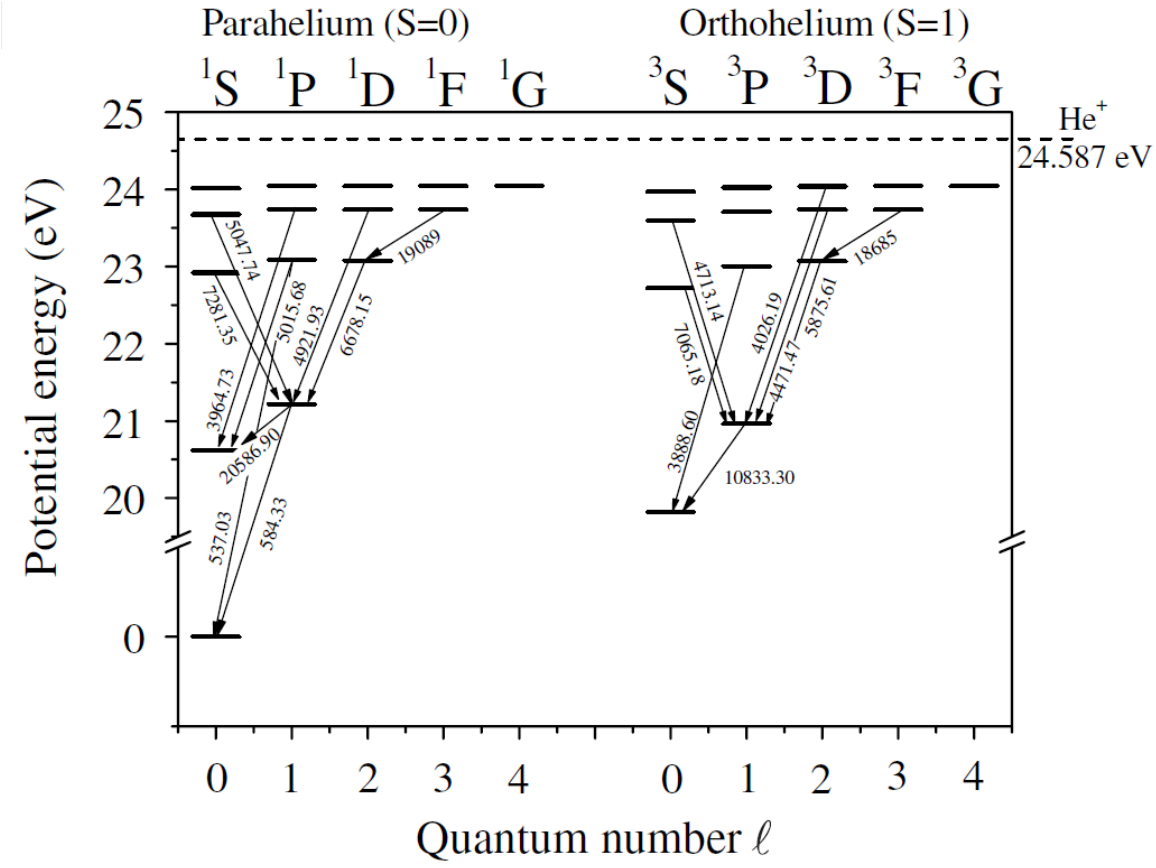

Figure 2: The potential energy levels of the excited states and ionized state of helium. Also, the radiative transitions with their corresponding wavelength in Å are illustrated. Figure from Belmonte et al. [3]

Quenching of the excited helium states He(2^1P) and He(2^1S) is proposed by Emmert et al. [12] for plasma pressures higher than 1 atmosphere. The reaction is

$$\mathrm{He(n, l, s)} + 2\mathrm{He} \longrightarrow 3\mathrm{He}. \tag{29}$$

They determined a rate coefficient for the He(2^1P) case as 1.8×10^{-31} cm^{6}s^{-1} and for He(2^1S) to 1.3×10^{-33} cm^{6}s^{-1}. The proposed quenching is not adopted in other works under atmospheric pressure conditions, because it is seen as unlikely [3].

2.2.2 Ionization and recombination

Ionization of helium atoms

If electrons have high enough energy, the inelastic collisions between electrons and atoms can lead to ionization of helium ground state or helium excited state atoms. The general reaction scheme is given by

$$\mathrm{He}(n,l,s) + \mathrm{e} \longrightarrow \mathrm{He}^+ + \mathrm{e} + \mathrm{e} \tag{30}$$

Just like elastic collisions, the rate coefficients can be calculated with the cross sections that correspond to the reaction. However, rate coefficients have also been calculated. An expression for k_r for the ionization of the helium ground state is [50]

$$k_r = 2.584 \times 10^{-12} T_e^{0.68} \exp\left(-\frac{2.854092 \times 10^5}{T_\mathrm{e}}\right), \tag{31}$$

while the expression for the ionization of the $n = 2$ states is

$$k_r = 4.661 \times 10^{-10} T_e^{0.6} * BR * \exp\left(-\frac{5.546 \times 10^4}{T_e}\right), \tag{32}$$

with again the BR since the ionization of each excited state has another probability.

Penning ionization

Another ionization process is called Penning ionization. During this process, an excited species collides with another (excited) species. One of the species is ionized since the excitation energy of one species exceeds the ionization potential of the other one [42]. When two excited helium atoms collide, the expression for this reaction is [3]

$$\mathrm{He}\,(n',l',s') + \mathrm{He}\,(n,l,s) \longrightarrow \mathrm{He}^+ + \mathrm{He} + \mathrm{e}. \tag{33}$$

This type of ionization produces hot electrons which affect the high-energy shape of the EEDF [2]. It is also responsible for the lifetime shortening of atoms in the metastable state [7] and happens mainly during the discharge afterglow [9].

Rate coefficients of the Penning ionziation processes

The rate coefficients of the Penning processes have been determined experimentally and will be discussed. A rate coefficient for the reaction between two triplet He(2^3S) helium atomic metastables is obtained by Deloche et al. [9] as $k_r = (1.5 \pm 0.3) \times 10^{-9}$ cm^{3}s^{-1} with a branching ratio of 0.30. The rate coefficient is retrieved from averaging the calculated values of k_r between a pressure range of 5 and 100 Torr. On the other hand, the rate coefficient is expected to be pressure independent [43]. The work of Deloche et al. is compared to other results from different authors and are in close agreement to each other, so in the order of 10^{-9} cm^{3}s^{-1}. One important note is that these works considered other multiple Penning ionization mechanisms for the destruction of metastables in order to determine the value of k_r. Considering only metastable destruction by the collision of two He(2^3S) atoms in a model can lead to an overestimation of k_r [9]. Another value of k_r is adopted in the work of Yuan and Raja [50], which is from Rauf and Kushner [36] with a plasma condition at around 100 Torr and deduced from the value of Deloche et al. [9]. Its value is $k_r = 2.7 \times 10^{-10}$ cm^{3}s^{-1}. Alves et al. [2] adopted a gas temperature dependent k_r in their work by the use of a reported value from Liegel et al. [27] and assumed the temperature dependence proposed by Phelps and Molnar [33]. This k_r is given by

$$k_r = 2.9 \times 10^{-9} * BR * \left(\frac{T_g}{300}\right)^{\frac{1}{2}}. \tag{34}$$

Belmonte et al. [3] deduced a rate coefficient from the time evolution decay of the number density of the excited species in the $n = 3$ state. This time evolution was found by optical emission spectroscopy. By determining the slope of the decay, the temperature dependence was found to be

$$k_r = BR * \frac{2.9 \times 10^{-9}}{T_{\mathrm{g}}^{0.5}}. \tag{35}$$

The problem of this deduced expression is that there is no possibility to give any branching ratio BR for the production of atomic ions. Santos et al. [38] fitted the data of Alves et al. [2], where T_g was 300 K, and Belmonte et al. [3], where T_g was 2450 K. This yields an expression of k_r given by

$$k_r = 2.9 \times 10^{-9} * BR * \left(\frac{T_{\mathrm{g}}(\mathrm{K})}{300}\right)^{-1.86}. \tag{36}$$

The rate coefficient of the Penning ionization between other excited states are unknown and therefore equations (34) to (36) are also used for these processes in the works of the formerly mentioned authors.

Recombination of ionized atoms

Recombination of He^+, so the reverse process of equation (30), only produces $He(2^3S)$ atoms according to Deloche et al. [9]. However, Emmert et al. [12] claims that, at their conditions from 0.5 bar to 8 bar, superelastic collisions can occur at the produced excited states resulting in multiple lower excited state species. They made the assumption that the He(n=2) levels are created with a certain probability according to their statistical weight [3]. The equation for k_r of the recombination is

$$k_r = 6.0 \times 10^{-20} * BR * \left(\frac{T_{\mathrm{g}}}{T_{\mathrm{e}}}\right)^{4 \pm 0.5}, \tag{37}$$

where BR from Emmert et al. is 0.19, 0.56, 0.06 and 0.19 for $He(2^1P)$, $He(2^3P)$, $He(2^1S)$ and $He(2^3S)$ respectively. Belmonte et al. [3] extrapolated the data from Deloche et al. [9] at a gas temperature of 300 K and their calculated electron temperature dependent k_r at a gas temperature of 2450 K equals

$$k_r = \frac{1.1 \times 10^{-14}}{T_{\mathrm{e}}^{4.5}} T_{\mathrm{g}}^{2.3}. \tag{38}$$

They could not deduce the corresponding branching ratios from their calculations. The recombination process is considered negligible due to fast conversion of He^+ into molecular helium via three body collisions [6]. This reaction will be described in Section 2.2.3.

2.2.3 Molecular helium creation and destruction

Multiple processes are present for the formation of molecular helium during a helium gas discharge, which are able to occur very rapidly at atmospheric pressure [16]. Most of the molecular helium species present during the discharge are excited dimers (excimers) and ionized dimers. These excimers have certain energy levels and since molecular helium consists of two helium atoms, these can have multiple rovibrational excited states. The notation for an excimer with these states is $He_2^*(v, J)$ where v is the vibrational state and J the rotational state [32].
The energy diagram of the excimers and excited atoms is illustrated in Figure 3. The excimers are bound in excited states but are unstable in the electronic ground state [10]. Therefore, their energy levels are at $n = 2$ or higher. The energy levels with $n = 3$ or higher are called excited excimer states or Rydberg states. These excimers have energy levels that are close to the ion energy level and are characterized by long lifetimes and large collisional cross sections [6]. A general notation for a Rydberg state excimer is He_2^{Ry}. Also, a slow incident electron on He_2^+ by purely electronic interactions leads to doubly excited molecules He_2^{**} [32]. The molecular ions He_2^+ are always formed in a highly excited rovibrational state [9, 32]. Molecular ions He_2^+ are the dominant

ions when the gas pressure is higher than 5 Torr at room temperature [9]. The molecular helium production and destruction processes are described in the following sections.

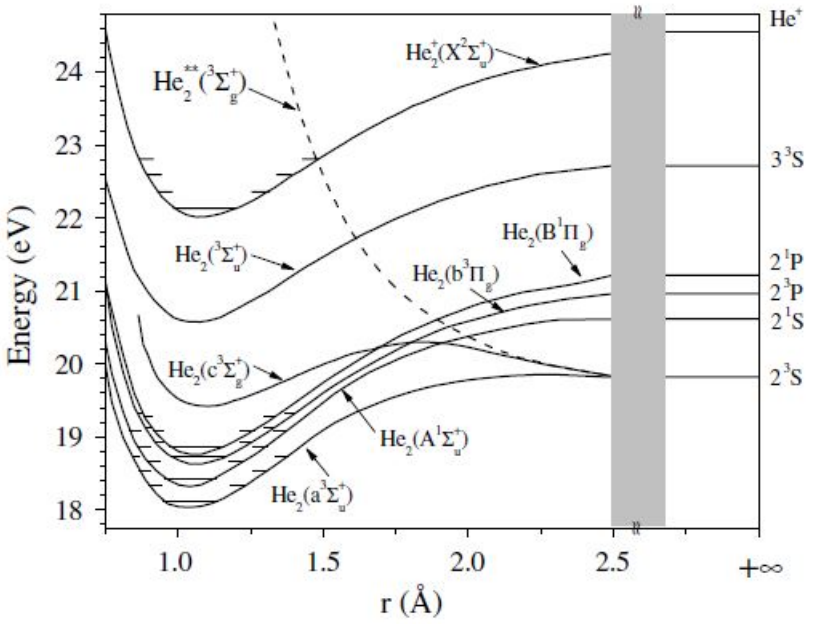

Figure 3: Illustration of the energy levels of the excimers, ionized dimer, excited helium atoms and ionized helium. The rovibrational states are illustrated by the short lines between the potential energy curves. Figure from Belmonte et al. [3].

Three-body collision resulting in molecular ions

The three-body collision is considered to be an important production channel of He_2^+ at atmospheric pressure conditions [2]. It is given by [3]

$$He^+ + 2He \longrightarrow He_2^+ + He. \tag{39}$$

The corresponding reaction rate is investigated by many authors and are all in the order of 10^{-32} to 10^{-32} cm^6s^{-1} [2]. Böhringer et al. [4] derived a temperature dependent k_r and is given by

$$k_r = 1.4 \times 10^{-31} \left(\frac{300}{T_g}\right)^{0.6\pm0.1} \tag{40}$$

as well as Russel [37], who derived k_r to

$$k_r = 0.86 \times 10^{-31} \left(\frac{T_g}{300}\right)^{-0.36\pm0.10}. \tag{41}$$

These equations are rather different while their experimental data differs by less than 30%. Probably, the accuracy of the measurements were not high enough to determine the exponent of the power law, according to Belmonte et al. [3]. The reversed reaction, which is called dissociation by atom impact, is also possible. A k_r is determined by Jonkers et al. where they used the principle of detailed balancing and a modified Saha equation [24]. k_r is given by

$$k_r = \frac{1.40 \times 10^{-6}}{T_g^{0.67}} \exp\left(-\frac{28100}{T_g}\right). \tag{42}$$

Three-body collision resulting in excimers

A production mechanism of excimers is the three body recombination of He(2^3S) or He(2^3P) with ground state He atoms, which is given by

$$\left\{ \begin{array}{l} \mathrm{He}\left(2^3\mathrm{P}\right) \\ \mathrm{He}\left(2^3\mathrm{S}\right) \end{array} \right. + 2\mathrm{He} \longrightarrow \mathrm{He}_2^* + \mathrm{He}, \tag{43}$$

where He_2^* is the abbreviated notation of an excimer that can have different energy states. In this case, the state can be either $\mathrm{a}^3\Sigma_\mathrm{u}^+$, $A^1\Sigma_u^+$ or $b^3\Pi_g$ state depending on the species involved. Neutral dimers are also created with high vibrational excitation. The temperature dependent k_r of the reaction with He(2^3S) involved is determined by Köymen et al. [25] which is

$$k_r = T_g \left[8.7 \exp\left(-\frac{750}{T_g} \right) + 0.41 \exp\left(-\frac{200}{T_g} \right) \right] \times 10^{-36}, \tag{44}$$

resulting in the excimer with the $\mathrm{a}^3\Sigma_\mathrm{u}^+$ state. A temperature dependent rate coefficient of the reaction with He(2^3P) is determined by Zhao et al. to [51]

$$k_r = \left(2.5 + 267 T_g^{-1} \right) \times 10^{-32}, \tag{45}$$

where the excimer is created with the $b^3\Pi_g$ state. Other values of k_r without a temperature dependence are determined. The value of the reaction with He(2^3P) involved is found to be 1.6×10^{-32} $\mathrm{cm}^6\mathrm{s}^{-1}$ with the excimer state $\mathrm{a}^3\Sigma_\mathrm{u}^+$ [12]. Golubovskii et al. [16] used the same value, but with the resulting excimer state $A^1\Sigma_\mathrm{u}^+$. This is probably a misunderstanding of the used source in their work, since this source is that of Emmert et al. who state that the $\mathrm{a}^3\Sigma_\mathrm{u}^+$ is involved. Another value of 1.3×10^{-33} $\mathrm{cm}^6\mathrm{s}^{-1}$ is adopted in the work of Yuan and Raja [50] for both reactions. A reversed process is proposed by Belmonte et al. since it is expected that the dissociation is efficient at temperatures in the order of 10^3 K. However, the reaction rate of this reversed process is unknown. Belmonte et al. [3] made therefore an estimation for k_r to a value of 1.6×10^{-14} $\mathrm{cm}^3\mathrm{s}^{-1}$. Reaction rates for the reaction with He(2^3S) involved are found to be around $k_r = 0.20 \pm 0.03$ $\mathrm{Torr}^{-2}\mathrm{s}^{-1}$ [9, 31]. This rate coefficient has also a certain temperature dependence, since it is expressed in the pressure p with unit Torr. In order to calculate it to the unit $\mathrm{cm}^6\mathrm{s}^{-1}$, the ideal gas law can be used:

$$pV = N k_b T_g, \tag{46}$$

with V the volume and N the amount of particles. The values have a typical order of 10^{-34} $\mathrm{cm}^6\mathrm{s}^{-1}$ at room temperature [3, 12].

Penning ionization

He_2^+ is also formed due to Penning ionization. The reaction is given by

$$\mathrm{He}\left(n', l', s'\right) + \mathrm{He}\left(n, l, s\right) \longrightarrow \mathrm{He}_2^+ + \mathrm{e}. \tag{47}$$

The equations for k_r are the same of that of equations (34) to (36) with a BR of 0.7. Another Penning ionization is the process where an excited $n = 2$ state collides with an excimer in the $\mathrm{a}^3\Sigma_\mathrm{u}^+$ state [3]:

$$\mathrm{He}(n, l, s) + \mathrm{He}_2^* \longrightarrow \left\{ \begin{array}{l} \mathrm{He}^+ + \mathrm{He} + \mathrm{He} + \mathrm{e} \\ \mathrm{He}_2^+ + \mathrm{He} + \mathrm{e} \end{array} \right. , \tag{48}$$

with a BR of 0.15 for the upper reaction and 0.85 for the lower one. It is weak at high temperatures, where high means temperatures higher than 10^3 K [3]. Emmert et al. [12] estimated the k_r to 1.5×10^{-10} $\mathrm{cm}^3\mathrm{s}^{-1}$ and Deloche et al. [9] calculated a value of $(2.5 \pm 1.5) \times 10^{-9}$ $\mathrm{cm}^3\mathrm{s}^{-1}$. Two excimers in the $\mathrm{a}^3\Sigma_\mathrm{u}^+$ state are able to collide and its reaction is given by

$$\mathrm{He}_2^* + \mathrm{He}_2^* \longrightarrow \mathrm{e} + \left\{ \begin{array}{l} \mathrm{He}^+ + 3\mathrm{He} \\ \mathrm{He}_2^+ + 2\mathrm{He} \end{array} \right. , \tag{49}$$

with a BR of 0.15 for the upper reaction and 0.85 for the lower one. The equation of k_r for this reaction from Claustre et al. is [7]

$$k_r = 1.5 \times 10^{-9} \left(\frac{T_g(K)}{300} \right)^{0.5}. \tag{50}$$

The expression of Claustre et al. is taken from Wang et al. [47], but differences between the equations are observed. The equation from Wang et al. equals that of expression (34). One possible reason is that an equation is derived where the energy dependence is taken from Wang et al. and combined to the value of 1.5×10^{-10} $\mathrm{cm^3 s^{-1}}$ found by Myers et al. [30]. Wang et al. adopted for all Penning reactions the reaction coefficient of Alves et al. [2], given by (34). The values of Myers et al. and Deloche et al. differ one order of magnitude. An explanation can be found in the article of Myers et al.

De-excitation of excimers

A superelastic de-excitation of $\mathrm{He_2^*}$ in the $\mathrm{a^3\Sigma_u^+}$ state to the ground state occurs and is very efficient for destroying metastable excimers at every pressure. It reads

$$\mathrm{He_2^* + e \longrightarrow 2He + e} \tag{51}$$

and its temperature independent rate coefficient is found to be 4.0×10^{-9} $\mathrm{cm^3 s^{-1}}$ [9]. An electron temperature dependent coefficient was first proposed by Deloche et al. but later suppressed by the same authors [3, 9].
Another mechanism turns $\mathrm{He_2^*}$ into $\mathrm{He_2^+}$ by electron collisions at room temperature:

$$\mathrm{He_2^* + e \longrightarrow He_2^+ + 2e}, \tag{52}$$

where an electron temperature dependent equation is given by [36]

$$k_r = 1.268 \times 10^{-12} T_e^{0.71} \exp\left(-\frac{3.945 \times 10^4}{T_\mathrm{e}} \right). \tag{53}$$

According to Belmonte et al, this mechanism is limited to low temperature plasmas where the density of neutral dimers is high.

Electron stabelized recombination

The reversed process of the de-excitation of excimers, namely electron-stabilized recombination, has also a branching to a metastable state:

$$\mathrm{He_2^+ + e + e \longrightarrow} \begin{cases} \mathrm{He}\left(2^3\mathrm{S}\right) + \mathrm{He + e} \\ \mathrm{He_2^* + e} \end{cases}. \tag{54}$$

This reaction is usually considered in the early afterglow of atmospheric pressure plasmas, under reduced pressure conditions or at high gas temperatures [7]. The formation of $\mathrm{He_2^*}$ is due to the production of doubly excited helium $\mathrm{He_2^{**}}$ which de-excites very rapidly to the metastable excimer with the $\mathrm{a^3\Sigma_u^+}$ state or the $\mathrm{A^1\Sigma_u^+}$ state. The last state decays by radiation to ground state helium [12]. According to Claustre et al. its branching ratio is 0.5, while according to Emmert et al. the branching ratio is 0.25 for the upper reaction and 0.75 for the lower one. Deloche et al. state that only $\mathrm{He}(2^3\mathrm{S})$ is formed just like stated in section 2.2.2. Its rate coefficient is given by [9, 12]

$$k_r = 4.0 \times 10^{-20} * BR * \left(\frac{T_\mathrm{g}}{T_\mathrm{e}} \right)^4. \tag{55}$$

Belmonte et al. used again recombination expression (38) for k_r since the reaction pathways dealing with atomic and molecular ions can be interchanged.
Direct dissociative recombination is also studied by many authors, which is

$$\mathrm{He_2^+ + e \longrightarrow He}(n, l, s) + \mathrm{He}. \tag{56}$$

The direct recombination creates first a doubly excited or Rydberg helium molecule, which eventually decays. This decay results in a branching to multiple excited helium atoms dependent on the initial rovibrational state of He_2^+. The efficiency of the dissociative recombination is dependent on the crossing of the energy levels of the doubly excited or Rydberg state helium and the rovibrational ionized helium state which can be seen in Figure 3 for the case of the doubly excited state [16, 32]. A competing process of the direct dissociative recombination is the auto-ionization of the doubly excited or Rydberg state back to the molecular ions, which is responsible for a reduction of the rate coefficient value [3, 8]. Pedersen et al. determined the branching ratios experimentally for the case when the lowest vibrational state of He_2^+ is involved. They are found to be $(3.7 \pm 1.2)\%$ for He(2^3S), $(37.4 \pm 4.0)\%$ for He(2^1S), $(58.6 \pm 5.2)\%$ for He(2^3P) and $(2.9 \pm 3.0)\%$ for He(2^1P). The total rate coefficient was found to be $(3.3 \pm 0.9) \times 10^{-10}$ cm^{3}s^{-1}. For higher vibrational levels, the rate coefficient was determined to be 2×10^{-7}cm^{3}s^{-1} or greater resulting in helium $n = 3$ states. Other authors have found or adopted an electron and gas temperature dependence of k_r like [2, 9]

$$k_r = 5.0 \times 10^{-9} \left(\frac{T_\mathrm{g}}{T_\mathrm{e}} \right)^{1 \pm 1}, \tag{57}$$

resulting only in He(2^3S) according to Alves et al. or 30% He(2^3P) and 70% He(2^3S) according to Deloche et al. Another rate coefficient is given by Golubovskii et al. [16] and reads

$$k_r = 8.9 \times 10^{-9} \left(\frac{T_\mathrm{g}}{T_\mathrm{e}} \right)^{1.5}, \tag{58}$$

with the metastable excited atom states as products.

Neutral-assisted recombination of molecular ions

Neutral-assisted recombination of He_2^+ is possible when the temperature is low enough, so in the room temperature regime. It is weak compared to the ambipolar diffusion process according to Belmonte et al. [3]. However, it is adopted in the work of Wang et al. [47] while considering ambipolar diffusion. The reaction is given by

$$\mathrm{He}_2^+ + \mathrm{He} + \mathrm{e} \longrightarrow \begin{cases} \mathrm{He}_2^{\mathrm{Ry}} + \mathrm{He} \\ \mathrm{He}(n,l,s) + 2\mathrm{He} \end{cases}. \tag{59}$$

The rate coefficients are found to be in the order of 10^{-27} cm^{6}s^{-1} [45]. Many calculations are done in the low-pressure regime where the value is considered independent of the pressure. On the contrary, van Sonsbeek et al. [45] stated that the rate coefficient is pressure dependent. Because the pressure dependence is not able to be resolved at low pressures, authors who worked with low-pressure plasmas mistakenly concluded that the experimentally determined rate coefficients are independent of the pressure. It was one of the reasons why the rate coefficients are subject to inaccuracies [45]. Van Sonsbeek et al. were able to deduce the total dissociation rate coefficient of the direct recombination and the three-body recombination at atmospheric pressure and a gas temperature of 295 K to

$$\alpha = (1.12 \pm 0.05) \times 10^{-7} + (2.20 \pm 0.25) \times 10^{-27} M, \tag{60}$$

with M the gas number density of ground state helium in cm^{-3} and α in cm^{3}s^{-1}. The first term in the expression is the rate coefficient of the direct recombination, while the second term is the rate coefficient of the three-body recombination multiplied by the gas number density. The total reaction rate of the dissociation of He_2^+ is proportional to α. A gas temperature dependence of (59) was also experimentally found to $T_g^{-2.9 \pm 1.2}$. From Sonsbeek et al., Belmonte et al. give k_r as

$$k_r = 1.60 \times 10^{-27} \left(\frac{T_\mathrm{g}}{300} \right)^{-2.9 \pm 1.2}. \tag{61}$$

The existence of the upper and lower channel in equation (59) are proposed and its existence is debated. Emmert et al. [12] adopted a direct recombination channel where He(2^3P) and He(2^3P) atoms are produced according to their statistical weight. Its k_r is

$$k_r = 1.0 \times 10^{-26} \left(\frac{T_\mathrm{g}}{T_\mathrm{e}} \right)^2 \tag{62}$$

and with using this k_r they achieved a good agreement between their experimental He(2^3P) temporal evolution and their theoretical He_2^+ evolution [6, 12]. However, the temperature dependence was adopted from Deloche et al. [9] who measured this dependence in the low pressure regime. This electron temperature dependence is measured for the two-body recombination and not for the three-body recombination [45]. Therefore, the adoption of the electron temperature dependence can be incorrect.
On the contrary, Schregel et al. [39] proved experimentally for the first time that molecular Rydberg states are produced. Carbone et al. [6] assumed the rate coefficient of this reaction from Sonsbeek et al. but with a different coefficient than Belmonte et al. [3]:

$$k_r = 2 \times 10^{-27} \left(\frac{T_g}{500} \right)^{-2.5} . \tag{63}$$

2.2.4 Radiation

An excited helium atom is able to decay by radiative transitions to another excited state or the ground state. The general expression for an allowed radiative electric dipole transition is

$$\mathrm{He}(n, l, s) \longrightarrow \mathrm{He}\,(n', l \pm 1, s) + h\nu \tag{64}$$

where h is Planck's constant and ν the frequency of the emitted photons with unit s^{-1}. The allowed transitions are illustrated in Figure 2. The electric dipole radiation is only permitted between two states if certain selection rules are met. If this is not the case, excited states can also decay by other radiative transitions. These transitions are generally much weaker, leading to transition time scales that exceed the collision time scales of the species. Excited species that are not able to decay by allowed transitions are called metastable atoms [26].
The rate of the radiative decay is called the radiative transition probability A_{ki}, where i and k stand for the higher and lower level respectively. The energy that is produced by this transition is the energy difference between the states and dissipates by radiation. The energy difference is given by

$$E_i - E_k = h\nu_{ik}, \tag{65}$$

where ν_{ik} the frequency of the emitted photons made from the decay between the states i and k [10]. Since the radiation produced from one transition has a certain wavelength λ_{ik}, the transitions can be observed by their corresponding spectral lines. The wavelengths of the radiative transitions are given in Figure 2. The rate of decrease of the population of species in a certain excited state due to radiative decay is given by

$$\frac{\mathrm{d}N_i}{\mathrm{d}t} = -A_i N_i, \tag{66}$$

where N_i is the population of excited atoms and A_i is the transition probability with unit s^{-1}. Several transition paths from E_i to E_k are illustrated in Figure 4. Please note that Figure 4 is a simplification of reality, because more transition paths to other lower energies are possible than illustrated. Also, the resulted exited atom in the lower energy level can eventually decay to other energy levels.

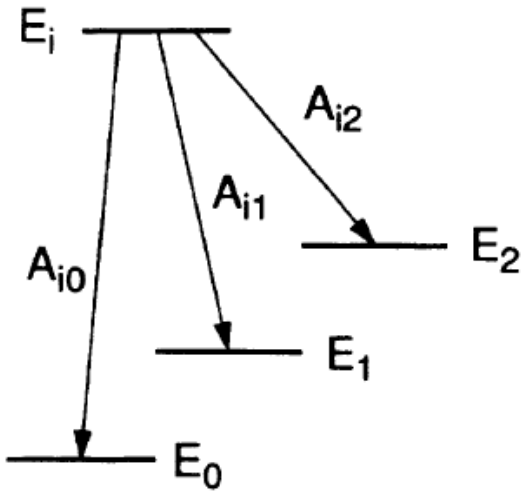

Figure 4: Illustration of multiple transitions from the energy state i corresponding to the energy of a certain excited state to lower energy states. Figure from Demtröder [10].

The total transition probability is then given by

$$A_i = \sum_k A_{ik}. \tag{67}$$

The values of A_{ki}, when allowed transitions are the considered, can be calculated from

$$A_{ik} = \frac{2\pi e^2}{m_e c \epsilon_0 \lambda^2} \frac{g_i}{g_k} f_{ki} = \frac{16\pi^3}{3h\epsilon_0 \lambda^3 g_i} S_{ki}, \tag{68}$$

where e is the electron charge, m_e is the electron mass, c is the speed of light and ϵ_0 is the permittivity of vacuum. g_k and g_i are the degeneracies of the excited states for the lower and higher energy respectively. f_{ki} is the oscillator strength and does not have a unit. f_{ki} is a useful measure to compare the strengths of the radiative transitions [22]. S_{ki} is the called the line strength and is given by

$$S_{ki} = |\langle \psi_k | P | \psi_i \rangle|^2, \tag{69}$$

where ψ_i and ψ_k are the initial and final wave functions respectively and P is the dipole operator [10, 28]. The radiative lifetime τ_i in seconds (s) of an excited state is given by

$$\tau_i = \frac{1}{A_i}. \tag{70}$$

Under certain plasma conditions, it is not assured that the radiation is able to escape to the walls directly. It is possible that the radiation is absorbed by another atom after the radiation had traversed a short distance, thereby raising the atom back to the originally excited state from the radiated atom. The emission and absorption of the radiation result merely in a transfer of excitation energy from atom to atom. The escape of this radiation to the walls may therefore require a large number of these transitions. The radiation is then called imprisoned [20]. Therefore, a unitless trapping factor g is defined in order to correct the lifetime of the excited states. This apparent lifetime is

$$\tau_{\text{app}} = \frac{\tau_0}{g}, \tag{71}$$

with τ_0 the natural radiative lifetime in seconds (s). The trapping factor is approximated to be

$$g \simeq g_0 T(\rho) \tag{72}$$

where the constant g_0 depends upon the absorption profile and trap geometry [29]. The probability $T(\rho)$ of the radiation travelling a distance ρ is given by

$$T(\rho) = \int P(\nu) e^{-k(\nu)\rho} d\nu, \tag{73}$$

where $P(\nu)$ is the frequency spectrum of the radiation emitted from a given volume element, ρ the travel distance of the radiation in m, ν the frequency in s^{-1} and $k(\nu)$ is the absorption coefficient in m^{-1}. $k(\nu)$ is a characteristic of the gas and has different forms when looking at the different types of absorption of the radiation in the gas. Since the atoms are in motion and have mutual interaction, frequency broadening of the absorption lines arises. One of these frequency broadening effects is Doppler-broadened absorption. The absorption is present when the Doppler shift, created by the motion of the particles, is large compared to the natural width. The other effect is pressure-broadened absorption, which results from the interaction between particles. The higher the pressure of the gas, the more important the pressure-broadening effect becomes. The expressions of $k(\nu)$ are determined for these two effects separately and with these two effects combined.
Holstein [20] derived the expressions for $T(\rho)$ for each effect based on the determined expressions of $k(\nu)$ and on the fundamental assumption

$$P(\nu) \propto k(\nu) \tag{74}$$

resulting in

$$T(\rho) = \frac{1}{k_0 \rho \left(\pi \ln(k_0 \rho)\right)^{\frac{1}{2}}} \tag{75}$$

for the case of Doppler-broadening and

$$T(\rho) = \frac{1}{\left(\pi k_d \rho\right)^{\frac{1}{2}}} \tag{76}$$

for pressure-broadening. An important note is that these equations are derived in the limit $k_0 \rho \gg 1$ and $k_d \rho \gg 1$. k_0 is the absorption coefficient at the line center in m^{-1} and is given by

$$k_0 = \frac{\lambda_{ik}^3 n_k}{8\pi} \frac{g_i}{g_k} \frac{1}{\pi^{\frac{1}{2}} v_0 \tau_{ik}}, \tag{77}$$

where n_k is the density of the absorbing atoms in the k state, τ_{ik} is the lifetime of the excited atom when looking at the transition from i to k and v_0 is the average particle velocity in ms^{-1}. The expression for v_0 is

$$v_0 = \sqrt{\frac{2k_b T_g}{m_h}}. \tag{78}$$

T_g is the temperature of the gas in K, k_b is the Boltzmann constant and m_h is the particle mass which is in this case the helium mass. k_d has the same definition as k_0 but has a different expression, namely

$$k_d = \frac{\lambda_{ik}^2 N}{2\pi} \frac{g_i}{g_k} \frac{\gamma}{\gamma_p}, \tag{79}$$

where γ is given by

$$\gamma = \frac{1}{\tau_{ik}} \tag{80}$$

and γ_d is

$$\gamma_{\mathrm{d}} = \frac{4e^2 f_{ik} \lambda_{ik} n_k}{3mc}. \tag{81}$$

The theory of Holstein [20, 21] is later extended by Walsh [46] and by Mills and Hieftje [29]. They derived an expression for the trapping factor g considering both Doppler and pressure broadening. The expression is

$$g_{ki} = g_{d_{ki}} \exp\left(-\frac{g_{cd_{ik}}^2}{g_{c_{ki}}^2}\right) + g_{c_{ik}} \operatorname{erf}\left(\frac{g_{cd_{ki}}}{g_{c_{ki}}}\right). \tag{82}$$

$g_{d_{ki}}$ and $g_{c_{ki}}$ are the partial escape factors for pure Doppler and for pure pressure broadening respectively and $g_{cd_{ki}}$ is the escape factor of the combined absorption spectral profiles. When a cylindrical geometry with a radius R is the case, the expressions for these quantities are given by

$$g_{d_{ki}} = \frac{1.60}{k_0 R \left[\pi \ln\left(k_0 R\right)\right]^{\frac{1}{2}}}, \tag{83}$$

$$g_{c_{ki}} = \frac{2}{\sqrt{\pi}} \left(\frac{\sqrt{\pi} a}{\pi k_0 R}\right)^{\frac{1}{2}}, \tag{84}$$

and

$$g_{cd_{ki}} = \frac{2a}{\pi \left[\ln\left(k_0 R\right)\right]^{\frac{1}{2}}}. \tag{85}$$

a is the unitless damping coefficient with the expression

$$a = \frac{\left(\gamma + \gamma_c\right) \lambda_{ik}}{4\pi v_0}. \tag{86}$$

The equation of the rate coefficient for radiation k_{rad} in s^{-1} can be derived from equations (70), (71) and (82) to

$$k_{rad} = g_{ki} A_{ik}. \tag{87}$$

The opacity range $k_r R$ must be large enough in order to have a real value of g_{ki}. It means that if the plasma with a certain radius R is not dense enough to let radiation trapping happen, radiation will fully escape and g_{ki} tends to go to 1.

3 Model description

A global model is developed with PLASIMO software to model the time dependent electron density and electron temperature from a plasma helium jet [11]. Its PLASIMO code can be found in Appendix A. Since a pure helium atmosphere is considered, only helium chemistry is involved in the model. The densities of the species are calculated according to the species balance given by equation (7). Ground state helium atoms, excited helium atoms with quantum number $n = 2$, helium excimers He_2^* in the lowest possible metastable state $a^3\Sigma_u^+$ and the molecular helium ions He_2^+ are present in the model. Discharges take place in proximity of a plasma needle of the plasma jet. It is considered that the needle is cylindrical with a radius of $R = 1$ mm and a length of $L = 5$ mm. The plasma is generated under atmospheric conditions, so the pressure is 1 atm. The initial density of the neutral helium atoms is $N/V = 2.25 \times 10^{25}$ m^{-3}. Furthermore, quasineutrality is assumed and there are no diffusion, drift or any form of transport processes present in the model. In the next sections, other properties of the model are discussed.

3.1 Energy balance

The energy balance of the electron temperature is calculated by equation (17). In this work, P_{in} is produced by a power P as a result of an applied alternating voltage U with an RF frequency f of 13.56 MHz and a certain current I. This frequency is commonly used for APPJs [49]. A phase difference θ between I and U is present. So P_{in} can be given by

$$P_{in} = IU \sin^2(2\pi f t + \theta) = P_{max} \sin^2(2\pi f + \theta), \tag{88}$$

where P_{max} is the maximum input power and is used as an input parameter of the model. The input power is pulsed. The power is turned on for the first 2 ms and turned off for 8 ms, so the total pulse width is 10 ms. In order to decrease the calculation time, the power input function is averaged over the time interval t_{on} which results in

$$P_{in} = \frac{1}{t_{on}} \int_0^{t_{on}} P_{max} \sin^2(2\pi f + \theta) dt = 0.5 P_{max} \tag{89}$$

which is a constant power input. So the input will look like a pulsed block function. This is illustrated in Figure 5. A typical value for a power input is $P_{in} = 10$ W. By dividing the power by the volume, the power density in the model can be calculated. Given the volume of the needle and $P_{in} = 10$ W, the power density in this case is $P_{in}/V = 3.18 \times 10^8$ Wm^{-3}.

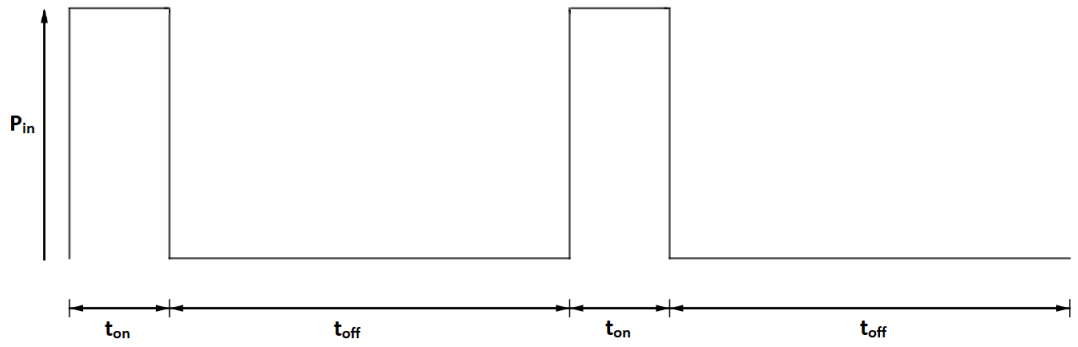

Figure 5: Simple illustration of the input pulse with averaging of the oscillating power. The pulse is turned on for a time of $t_{on} = 2$ ms and turned off for a time of $t_{off} = 8$ ms repeatedly.

During the time the power is turned on, the gas is able to heat up. This results in a higher T_g which therefore can affect the gas temperature dependent rate coefficients. It is considered that most of the heating process is due to elastic collisions [3, 38]. However, there was no possibility to

implement the gas temperature change in the model with the used software. The gas temperature is therefore considered constant with a value of T_g=300 K. The gas temperature dependence of the rate coefficients is still considered as important for further implementation when the gas heating feature is added to the software.

3.2 Plasma chemistry for the model

As discussed in Section 2.2 several reactions are present in the helium discharge. However, the presence of some of these reactions are debated. Also, the adopted or derived rate coefficients from different authors differ. The used reactions with the adopted rate coefficients are discussed in the following sections. Each kind of process is discussed per section. Some rate coefficients of the electron-involved reactions are calculated by the use of cross sections. These reactions will be discussed in Section 3.2.5. The cross sections of some of the electron-involved reactions are unknown. Therefore, derived rate coefficients are adopted instead.

3.2.1 Ionization

The Penning processes $\mathrm{He}(n',l',s') + \mathrm{He}\,(n,l,s) \rightarrow \begin{cases} \mathrm{He}^+ + \mathrm{He} + \mathrm{e} \\ \mathrm{He}_2^+ + \mathrm{e} \end{cases}$,
$\mathrm{He}_2^* + \mathrm{He}_2^* \rightarrow \mathrm{e} + \begin{cases} \mathrm{He}^+ + 3\mathrm{He} \\ \mathrm{He}_2^+ + 2\mathrm{He} \end{cases}$ and $\mathrm{He}(n,l,s) + \mathrm{He}_2^* \rightarrow \begin{cases} \mathrm{He}^+ + \mathrm{He} + \mathrm{He} + \mathrm{e} \\ \mathrm{He}_2^+ + \mathrm{He} + \mathrm{e} \end{cases}$ are added to the model. When an excited state helium atom is involved, all possible Penning reactions between the excited states with quantum number $n = 2$ are considered. The adopted rate coefficient for the Penning process between two excited atoms is (36) with a branching ratio of 0.30 for the upper reaction and 0.70 for the lower reaction as adopted in the work of Santos et al. [38]. It provides an assumption of the combined rate coefficients given by (34) and (35) for the model as well as the assumption that the Penning ionziation processes have the same rate coefficients. An exception is the adopted rate coefficient of the reaction between two He_2^* excimers. It contains the derived rate coefficient at atmospheric pressure, which is the same pressure condition as in the model. The ionization of neutral dimers according to $\mathrm{He}_2^* + \mathrm{e} \rightarrow \mathrm{He}_2^+ + 2\mathrm{e}$ is also considered, assuming that its density is high enough and the gas temperature is low enough compared to the conditions in Belmonte et al. [3]. Its adopted rate coefficient is given by equation (53). The other ionization processes are discussed in Section 3.2.5.

3.2.2 Recombination

The electron assisted recombination of He^+, $\mathrm{He}^+ + \mathrm{e} + \mathrm{e} \rightarrow \mathrm{He}(n,l,s) + \mathrm{e}$, is neglected in this work since its rate coefficient is much lower than other destruction processes of He^+, which will be described in Section 3.2.3. On the other hand, electron assisted recombination of He_2^+, given by $\mathrm{He}_2^+ + \mathrm{e} + \mathrm{e} \rightarrow \begin{cases} \mathrm{He}\left(2^3\mathrm{S}\right) + \mathrm{He} + \mathrm{e} \\ \mathrm{He}_2^* + \mathrm{e} \end{cases}$, is not negligible. Following the assumptions of Belmonte et al. [3], equation (38) for k_r is adopted. Since the branching ratios are unknown, a branching ratio of 0.5 is used just like Santos et al. [38] did in their work. The products of the three-body recombination (59) are debated as mentioned in Section 2.2.3. Notwithstanding, it is evident that this reaction is present especially at the given helium density in this model when looking at equation (60) [45]. The reaction products in this model are produced according to Emmert et al. [12], following reaction $\mathrm{He}_2^+ + \mathrm{He} + \mathrm{e} \rightarrow \mathrm{He}(n,l,s) + 2\mathrm{He}$. It is branched to the excited states $\mathrm{He}(2^3\mathrm{P})$ and $\mathrm{He}(2^3\mathrm{P})$ with a branching ratio of 0.75 and 0.25 respectively. Equation (61) for k_r is adopted.

3.2.3 Other production and destruction mechanisms of molecular helium

The three-body collision $\mathrm{He}^+ + 2\mathrm{He} \rightarrow \mathrm{He}_2^+ + \mathrm{He}$ is used in the model and can be seen as the dominant destruction mechanism of He^+ because of the atmospheric pressure. A corresponding

k_r according to equation (40) is adopted. Dissociation by atom impact, $He_2^+ + He \rightarrow He^+ + 2He$, is neglected since equation (42) will become very small ($\sim 10^{-42}$ cm^3s^{-1}) compared to the other destruction mechanisms of He_2^+ by filling in the gas temperature condition used in this model. If the model is updated with the gas temperature change feature, it could be considered to adopt this reaction if the gas temperature rises to an order of 10^3 K.
Excimer creation by the three-body reaction, $\left\{ \begin{array}{l} He\left(2^3P\right) \\ He\left(2^3S\right) \end{array} \right. + 2He \rightarrow He_2^* + He$, is also included in the model. The gas dependent rate coefficients (44) and (45) are used. The produced excimers with state $b^3\Pi_g$ are quickly formed by radiative decay to the $a^3\Sigma_u^+$ state by a rate coefficent of $\sim 10^7 s^{-1}$ [16]. It is thus assumed that this reaction is faster than possible other reactions with the $b^3\Pi_g$ state excimers or the reactions with the $a^3\Sigma_u^+$ state excimers involved. When looking at a constant gas temperature of 300 K, these coefficients are in the same order of the other gas independent coefficients. Dissociation of excimers, given by $He_2^* + e \rightarrow 2He + e$, is added to the model since it is seen as an important destruction process of excimers. The given value of 4.0×10^{-9} cm^3s^{-1} is used. It was also adopted in the work of Belmonte et al. [3], Emmert et al. [12] and Hill and Hermann [19].

3.2.4 Radiative decay and quenching

Radiative decay of the following allowed transitions between excited states are added to the model: $He(2^3P) \rightarrow He(2^3S)$, $He(2^1P) \rightarrow He(2^1S)$ and $He(2^1P) \rightarrow He$. Their transition probabilities are used as rate coefficients in the model and are 1.0216×10^7 s^{-1}, 1.9746×10^6 s^{-1} and 1.7989×10^9 s^{-1} respectively. These values are taken from Wiese and Fuhr [48]. Because expression (82) for radiation trapping is too complex to be implemented in the software, there was no ability to add it. As a consequence, it is assumed that the gas is not dense enough to let radiation trapping happen and it will be neglected in this work.
Quenching is neglected in this work. The pressure in this model is assumed to be low enough that this will not occur, following the work of many authors who did the same like Belmonte et al. [3].

3.2.5 Electron-involved reactions

The rate coefficients of the reactions $He + e \rightarrow He + e$, $He(n,l,s) + e \leftrightarrow He\,(n',l',s') + e$, $He(n,l,s) + e \rightarrow He^+ + e + e$ and $He_2^+ + e \rightarrow He(n,l,s) + He$ are calculated by the use of equation (15). Energy dependent cross sections are used, which are added to the model by the input of a look-up table. The EEDF is calculated by solving the homogeneous two term approximation of the Boltzmann equation with the program BOLSIG+ [18]. The cross sections are derived by Santos et al. [38] and are partly taken from from the IST-Lisbon database [1] via LXCat [34]. However, the database was not complete so the remaining cross sections were taken from supplementary data file in the article of Santos et al. [38]. The cross sections used for equation (56) are deduced by Santos et al. [38] from the results of Pedersen et al. [32] and the derived branching ratios discussed in Section 2.2.3 are used in the model as well. These branching ratios are assumed to be energy independent and are therefore taken in the EEDF. As stated in Section 2.1, the ratios are thus multiplied with the cross sections in the look-up table. To use these cross sections, it must be assumed that the rovibrational states of He_2^+ decay faster to the lowest rovibrational state than that these excited He_2^+ molecules recombine. Because reactions of the excited atoms (26) have a certain equilibrium with their reversed process, detailed balancing is applied according to equation (12). Some of the superelastic de-excitation reactions are not seen as physically present in the model, but a modified rate coefficient of the inelastic excitation process is calculated by extracting the calculated rate coefficient of the de-excitation process from the rate coefficient of the excitation by the use of detailed balancing.
It is expected that excited helium atoms with the quantum number $n = 3$ or higher are present in the helium plasma [3]. In order to keep the model simple, these particles are not implemented in the model. However, the corresponding excitations of these helium atoms could change the shape of the EEDF. Therefore, cross sections of the excitations of excited helium atoms in the

state $n = 3$ or higher are added in the Boltzmann equation solver in order to calculate a more accurate EEDF. Unfortunately, there was no ability to plot the EEDF to find the role of these cross sections in the EEDF.

4 Results and discussion

In this section, results of the electron density and electron temperature are shown with the parameters described in section 3. In addition, these parameters are also tuned in order to have a look at the behavior of the model to these changes. Besides making a plot of the electron density and electron temperature, the PLASIMO software has other features which are used to give a better understanding of the model and the chemistry involved. The results from the parameter changes as well as the plots from the used PLASIMO features are discussed. The input power is chosen to be $P_{in} = 10$ W, except when the power is changed. This is the case in Section 4.3. The power density is $P_{in}/V = 3.18 \times 10^8$ Wm^{-3}.

4.1 Electron temperature and electron density

The electron temperature for the first two pulses are plotted in Figure 6. What can be observed is a large peak of the electron temperature at the beginning of the pulse. A small amount of electrons is present in the plasma before the power is turned on. These electrons gain energy when the power is turned on. The electron temperature rises since the energy is divided over a small amount of electrons, resulting in a large increase of the electron temperature. The induced chemical reactions produce electrons, which means that the energy will be divided over more electrons. This results in a drop of the electron temperature right after it had risen. After the peak, the electron temperature stays constant at a value of around 2.7×10^4 K. A difference between the increase of the electron temperature at the first pulse and the second pulse is observed. The reason of this difference is because of the first calculations of the electron temperature that are based on chosen input parameters. These values are chosen arbitrarily in the range where the solver of the software is able to make these calculations. After some iterations of the solver, the initial values for the next pulse change. The graphs of the electron temperature for the pulses after the second pulse do not change in shape. The peak of the electron temperature of the second pulse has a duration of about 50 µs. The electron temperature drops with a certain bump, as can be observed in Figure 7. A quick drop of the electron temperature is observed when the power is turned off. This drop happens with a duration of about 6 µs to a temperature of around 450 K for the second pulse. After the quick drop, a slower drop will follow to a electron temperature that is slightly higher than the gas temperature during the time the power is turned off. This drop is illustrated in Figure 8.

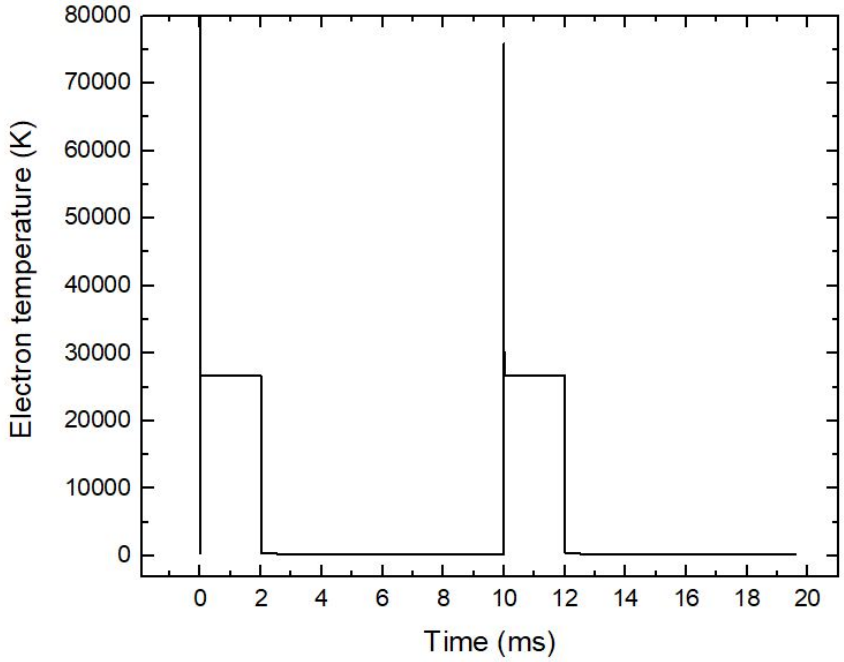

Figure 6: Plot of the electron temperature for the first two pulses calculated by the PLASIMO software. A quick increase followed by a decrease can be observed at the beginning of the pulse, as well as the differences of these increases for the two pulses.

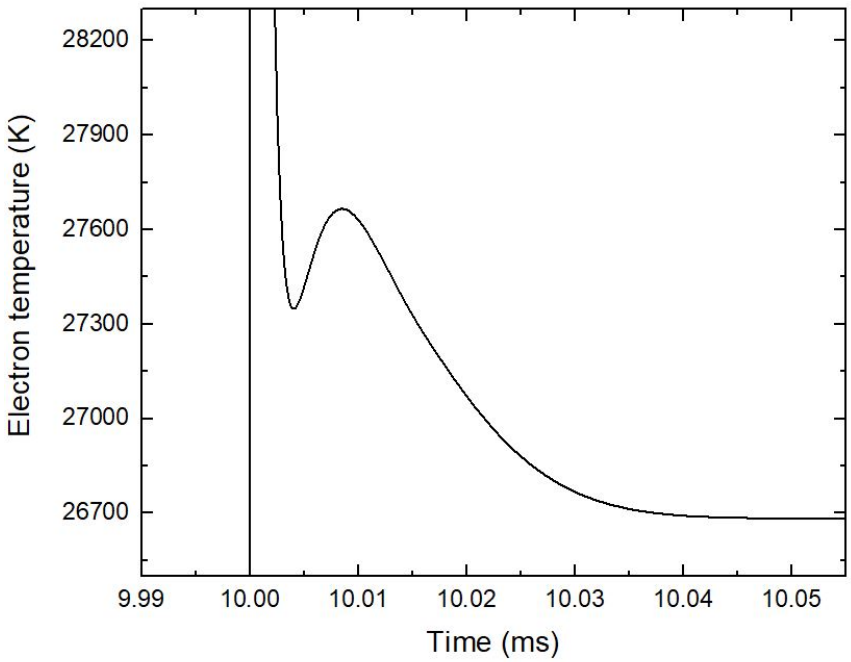

Figure 7: A part of the peak of the electron temperature at the moment the power is turned on is illustrated in this figure. A bump in the decay of the electron temperature can be observed.

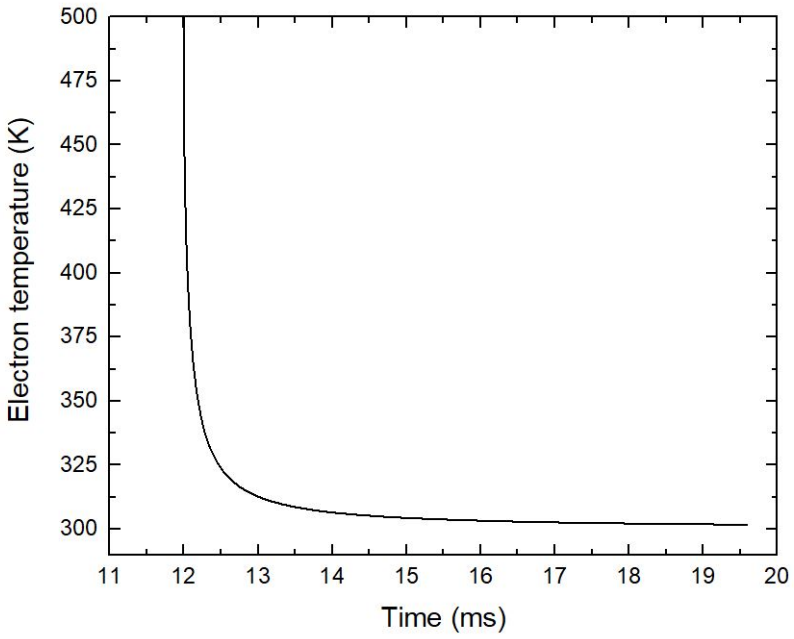

Figure 8: Plot of the slow drop after the quick drop of the electron temperature. The electron temperature will almost reach the gas temperature during the time the pulse is off.

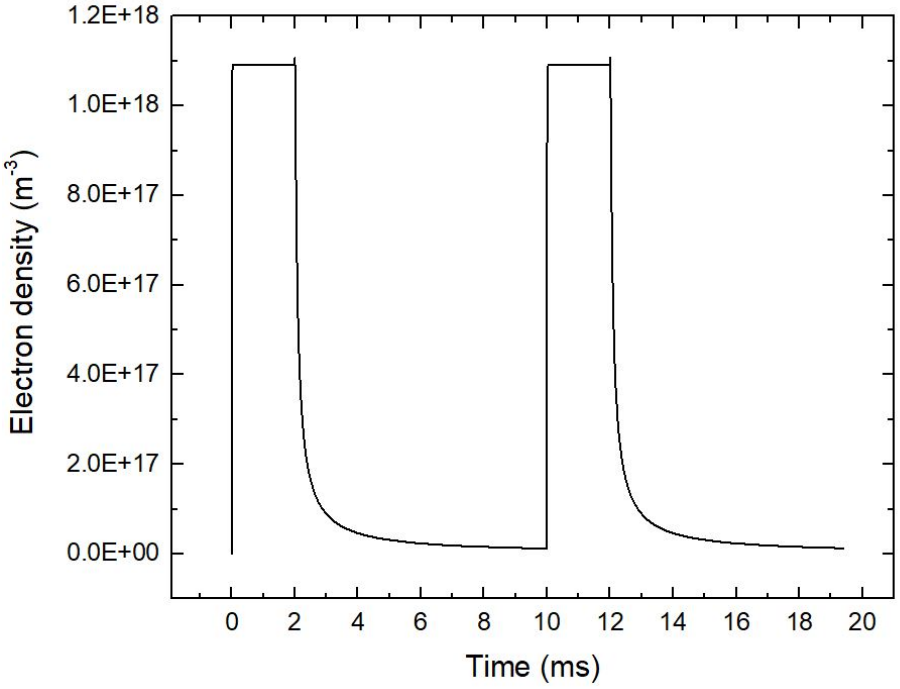

Figure 9: Plot of the electron density of the first two pulses. When the power is turned off, a small bump can be observed.

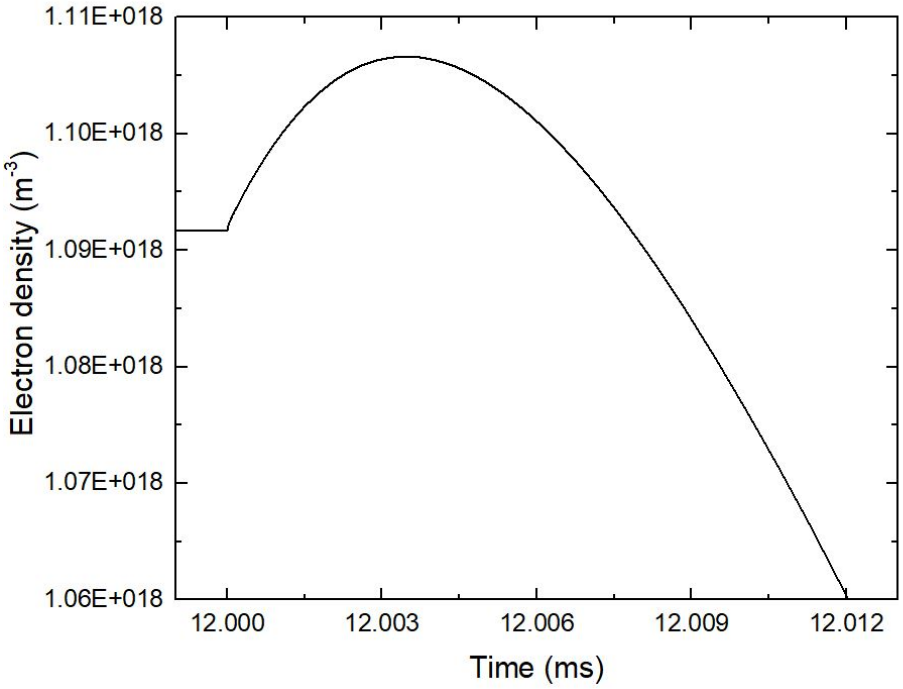

Figure 10: Plot of the the bump of the electron density at the moment when the power is turned off.

The plot of the electron density for the first two pulses can be seen in Figure 9. The electron density will rise to a value of 1.1×10^{18} m^{-3} in a time of around 40 µs for both pulses. When the power is turned off, a small bump can be observed. After the bump, the electron density decreases until the next pulse is turned on. This bump is illustrated in Figure 10. Note that the electron density does not decay completely before the next pulse starts. The electron density does not change when the power is turned on for each pulse, so there is no accumulation or reduction of the electrons.

4.2 Electron sources

The PLASIMO software is able to make a plot of the electron sources. The reactions that increase or decrease the electrons at a certain time can be investigated from these plots. A plot of some of the dominant destruction and production mechanisms of electrons during the steady state is illustrated in Figure 11. The ionization of the excited species $He(2^3S)$ has a high contribution to the electron production at the moment when the power is turned on. A balance between the production and destruction reactions lead to a steady state of the electron density. It can be observed that the Penning ionization process with two excimers He_2^* involved resulting in molecular ions He_2^+, given by the upper reaction in equation (49), is the most dominant production mechanism of electrons during the steady state. The ionization of ground and excited states of helium, as well as the dissociation of excimers to molecular ions given by equation (52) are present as well, but each have a contribution of less than 15% to the electron production. The main destruction mechanism during this time is the helium atom assisted recombination of He_2^+, given by the lower reaction in equation (59). This reaction produces $He(2^3P)$ atoms. The helium atom assisted recombination is around 55% responsible for the total recombination of He_2^+ during the steady state, while around 45% is due to the direction recombination of He_2^+. After the power is turned off, Penning processes are getting stronger as well as the helium atom assisted recombination processes and the electron assisted recombination reaction given by equation (56). The direct recombination processes of He_2^+ disappear when the power is turned off. The observed bump in the electron density is due to

the sharp increase of the Penning ionziation with the two excimers when the power is turned off. This electron production increase is, together with the increase of the other Penning processes, stronger than the destruction processes on the moment the power is turned off.

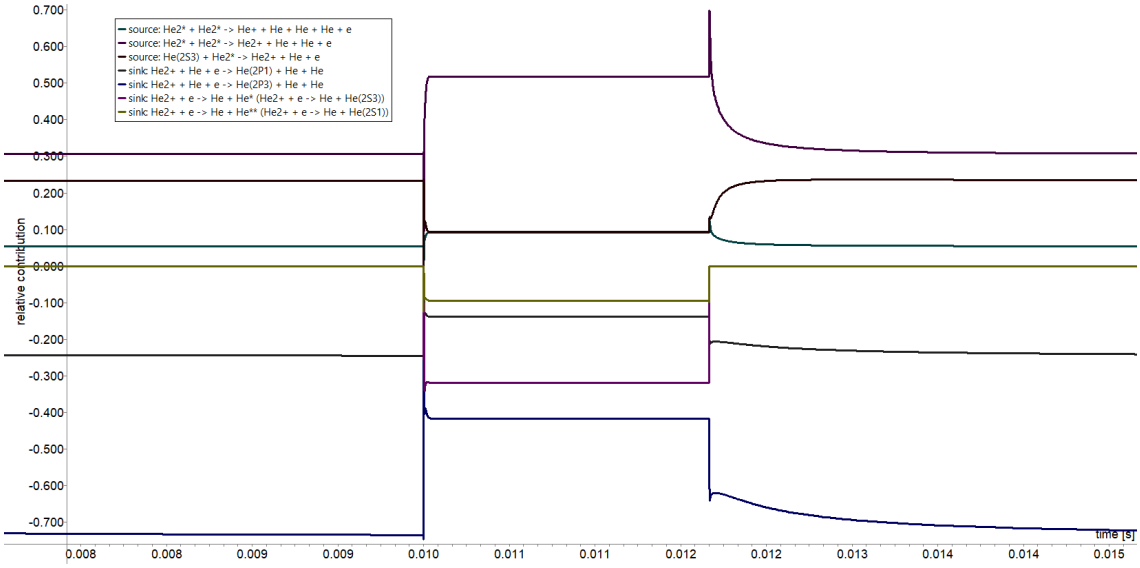

Figure 11: Plot of the main production and destruction mechanisms of electrons during the steady state. The plot is visualized by the PLASIMO software. A bump of the electron production contribution is observed for the Penning ionziation between two excimers when the power is turned off. The increase of the electron destruction from the helium atom assisted recombination and the decrease of the direct recombination of molecular ions can also be observed in this plot.

4.3 Power change

The input power is tuned over a range between 1 W and 1000 W to give a look at the density change of the excited and ionized species. The densities are taken from the steady state of the second pulse at $t = 11$ ms. The plot is given in Figure 12. The density of the atomic helium ions show a big increase of 5 orders of magnitude in the given power range. An explanation for this is that the electrons get sufficient energy to ionize the ground state helium. This ionization will therefore become more dominant compared to the ionization of excited helium, which have a lower density compared to ground state helium. A significant increase of the power also leads to a stronger increase of the excited helium atoms in the P states compared to that of the S states. The electron temperature is also plotted for different input powers in the time span of the second pulse. Again, a constant electron temperature is reached but these constant electron temperatures increase with power. This is illustrated in Figure 14.
The relative density of He_2^+ to that of He^+ is plotted and given in Figure 13 in order to give a better illustration of the relative increase. The density of He_2^+ is still the dominant ion in this power regime.

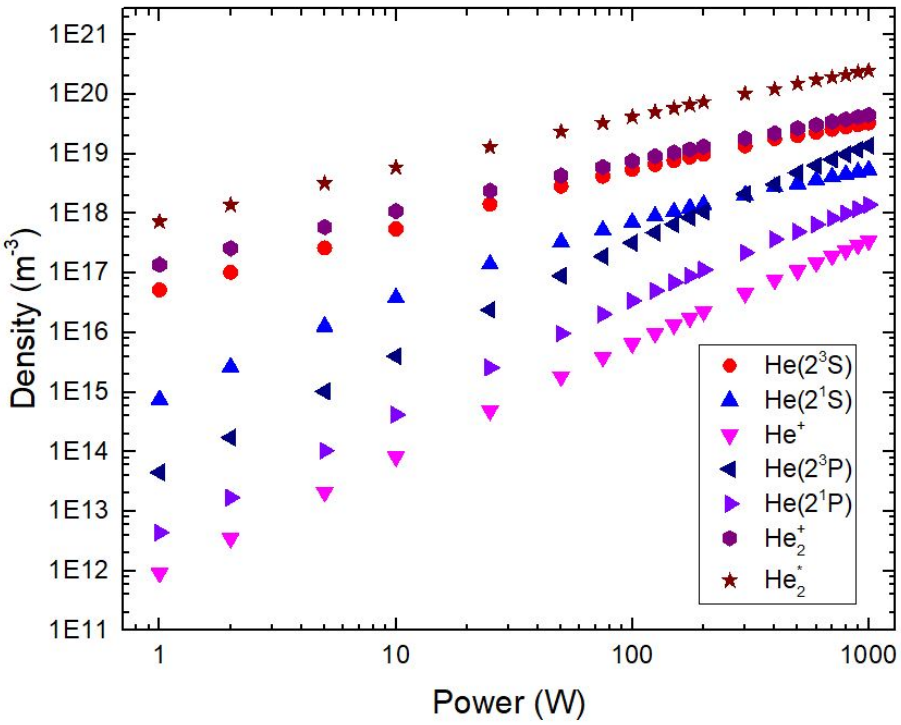

Figure 12: Logarithmic plot of the densities of the excited and ionized atoms and molecules for different power inputs. The electron density equals the He_2^+ density, since He_2^+ is the dominant ion in the plasma and quasineutrality is assumed.

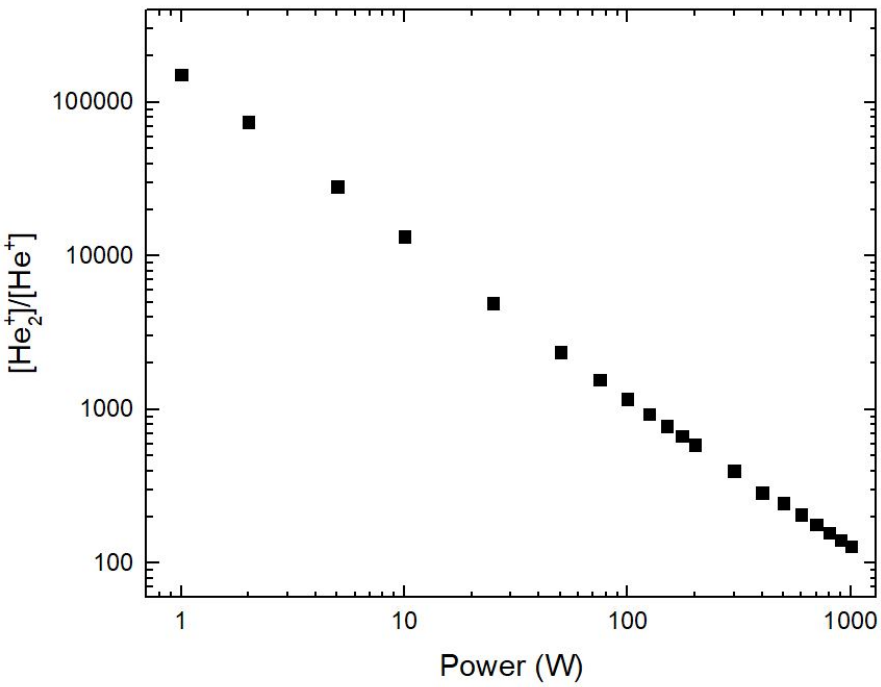

Figure 13: Logarithmic plot of the relation between the relative density of molecular ions and atomic ions and the power.

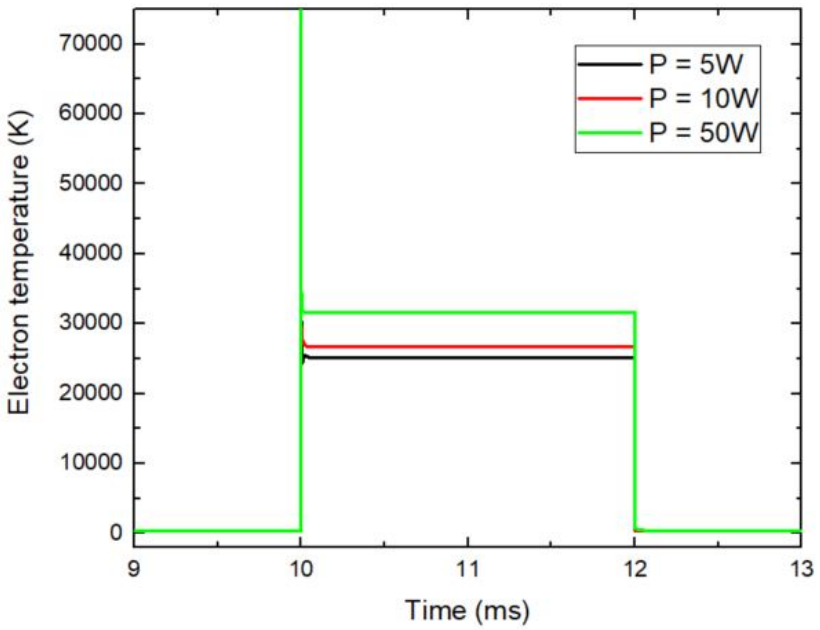

Figure 14: Plot of the electron temperature during the second pulse with different input powers.

4.4 Pressure change

The pressure is tuned by changing the amount of ground state helium atoms in order to find the densities of the ionized atoms and ionized molecules. The densities are taken from the steady state of the second pulse at $t = 11$ ms. The result is plotted in Figure 15. As stated in Section 2.2.3, the molecular helium ions are the most dominant ions above 5 Torr according to Deloche et al. [9]. However, the plot shows that the molecular helium ions have found to be dominant when the density of the helium ground atoms is above approximately 1×10^{24} m^{-3} following this model. When applying equation (46), this comes down to a pressure of around 40 Torr. As found in the previous section, the density of the molecular and atomic ions increase differently when the power is raised. So according to the model, the power also determines which ions are dominant in the discharge at a given pressure. The result is made with a constant power of 10 W.

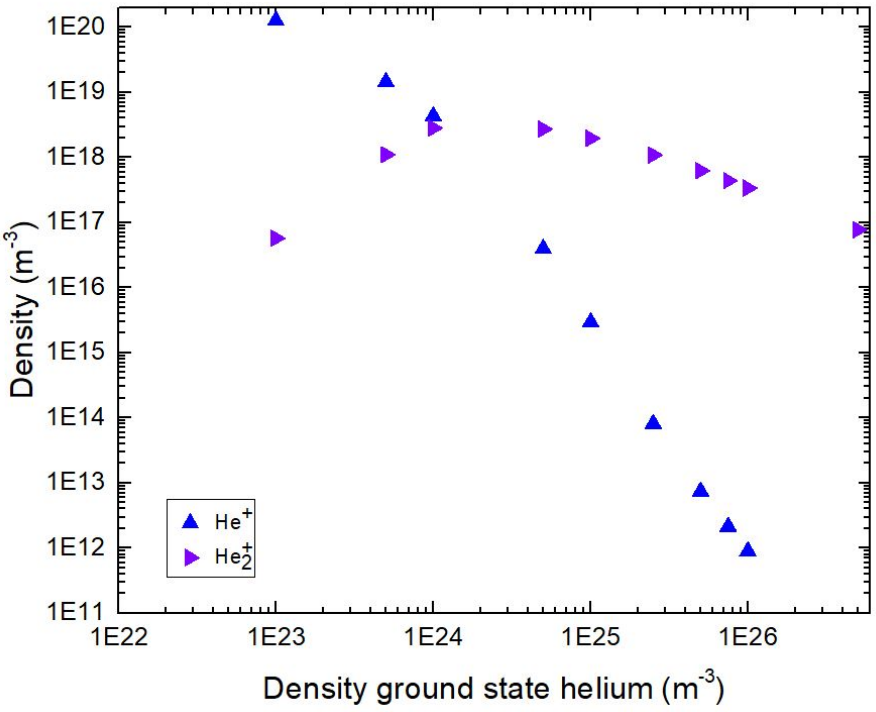

Figure 15: Logarithmic plot of the ion densities as a function of the ground state helium density. A change in ground state helium density means also an increase of pressure according to the ideal gas law.

4.5 Temperature change

A constant gas temperature is used in the model. However, this gas temperature can change in time according to the energy balance equations described in Section 2.1.2. Electrons give their energy to the heavy particles by collisions and therefore the gas temperature can increase. The PLASIMO software is able to plot the power density sources for electrons and heavy particles. An example of a power density source plot for electrons is illustrated in Figure 16. During the time the power is turned on, the input power is mainly lost due to elastic collisions. Only 0.08% is lost due to inelastic collisions. A temperature difference can be calculated from the plot and is found to be $\Delta T = 1.4 \times 10^3$ K. However, it is assumed that no energy is lost to the walls in this calculation. The difference is therefore expected to be lower. More importantly, an increase means that the rate coefficients can change in time. Some reactions can get more dominant in time and so the electron density could look very different than the plotted one in Figure 9.

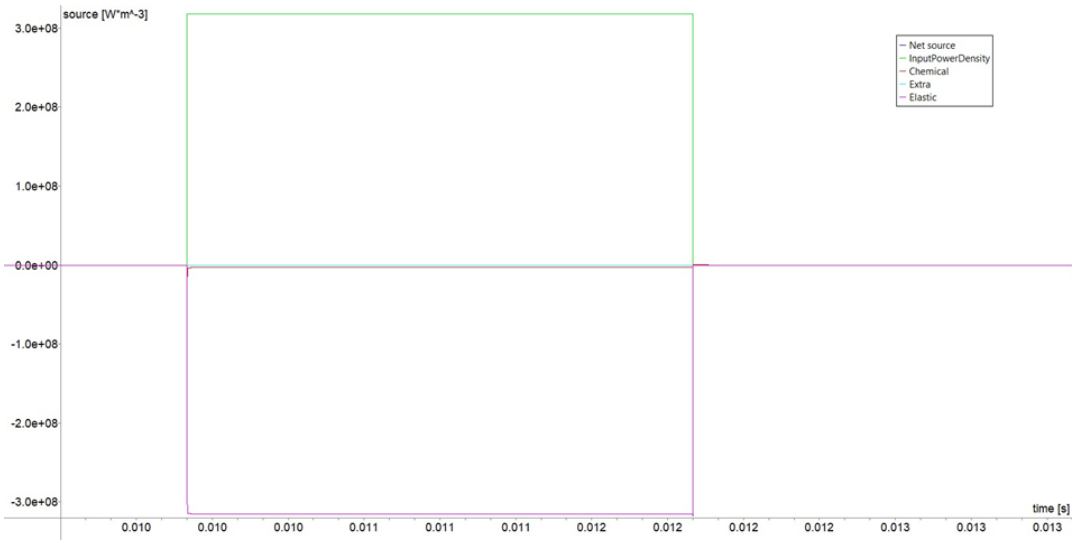

Figure 16: Plot of the power density source in the PLASIMO interface.

4.6 Rate coefficient change

As discussed in Section 2.2.3, multiple products and rate coefficients of equation (59) are proposed. This model adopts the rate coefficient given by $k_r = 1.60\times10^{-27}\left(\frac{T_g}{300}\right)^{-2.9\pm1.2}$. The rate coefficient is changed to the rate coefficient given by $k_r = 1.0\times10^{-26}\left(\frac{T_g}{T_e}\right)^2$ in order to see how the choice of a rate coefficient can affect the species densities. The densities of $He(2^3S)$, He_2^+ and He_2^* are plotted in the time span of the second pulse. These plots can be seen in Figure 17 for the different values of k_r. What can be observed is a significant difference between the two excimer densities. Also, the density of $He(2^3S)$ is slightly higher when equation (61) is adopted compared to the adoption of equation (55). On the contrary, the denisty of He_2^+ is slightly higher when equation (61) is adopted. However, the behaviors of the density decay look the same. The difference between the rate coefficients is the electron temperature dependence. It should be expected that during the quick drop of the electron temperature, the recombination of He_2^+ will be faster when equation (55) is adopted. It looks like this is not the case. A bump of the $He(2^3S)$ density is observed when the power is turned off. This bump is higher when equation (55) is adopted. This means that more $He(2^3S)$ is created during the time the power is turned off. The reaction creates $He(2^3P)$ and $He(2^1P)$, but these excited helium atoms decay very rapidly to $He(2^3S)$ or $He(2^1S)$. Due to the high increase of $He(2^3S)$, Penning ionization processes with $He(2^3S)$ and He_2^* involved become important processes. These processes create He_2^+ and this is probably why the decrease of He_2^+ does not decrease more rapidly if there is an electron temperature dependence in the k_r. Note that these processes have the same effect on the electron density as on the He_2^+ density. The electron density equals the He_2^+ density, since He_2^+ is the dominant ion and quasineutrality is assumed.

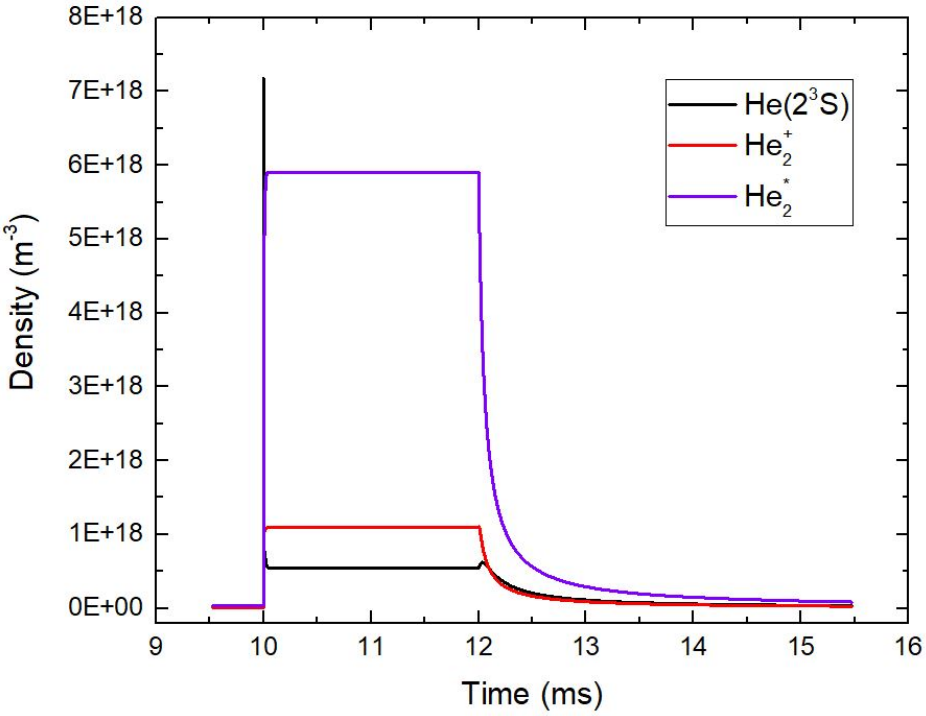

(a) k_r according to equation (61).

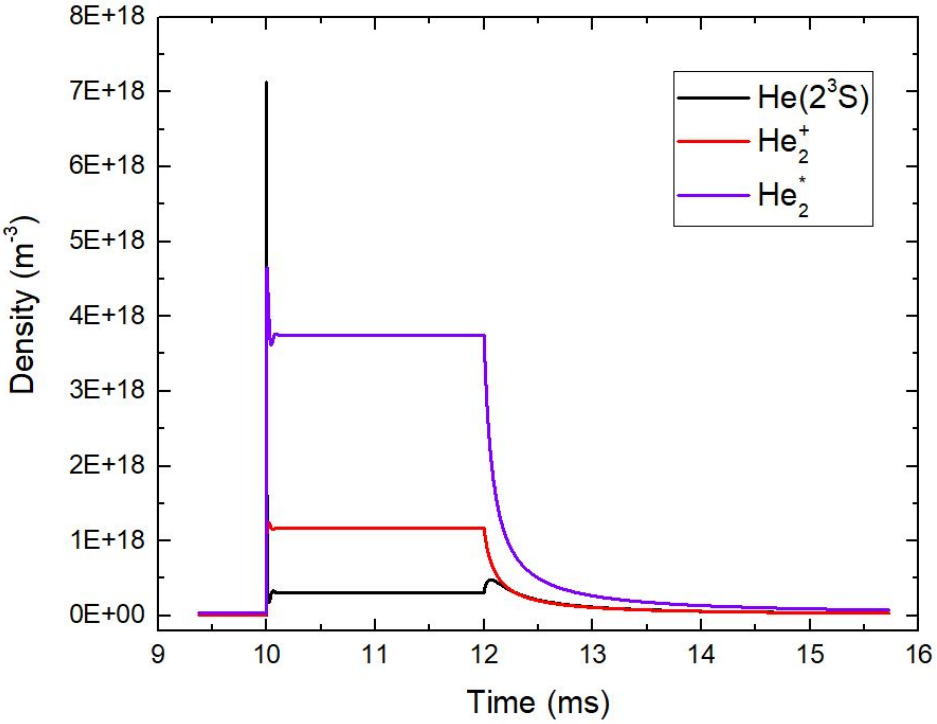

(b) k_r according to equation (55).

Figure 17: Plots of the densities of He(2^3S), He_2^+ and He_2^* during the second pulse for two different values of k_r.

4.7 Adding excimer dissociation

Lastly, a reaction is added to the model which initially was not added to the model before. It is the reversed process of the reaction given by equation (43), which is called excimer dissociation. Its rate coefficient is unknown and the process is considered to be efficient when the temperature is in the order of 10^3 K. In Section 4.5 it is mentioned that there is a significant increase of temperature leading to a gas temperature of the same order. Therefore, this reaction is also added to the model with the proposed k_r with the value 1.6×10^{-14} cm^3s^{-1}. Some of the excited densities are plotted as a function of time during the second pulse. This is illustrated in Figure 18. Adding the reaction leads to a decrease in He_2^* and an increase of $He(2^3S)$ compared to the densities retrieved from the model plotted in Figure 17a. The excited states $He(2^1S)$ and $He(2^3P)$ are also more present. The decrease of He_2^* is much steeper and there is a large bump of the $He(2^3S)$ density when the power is turned off. The Penning ionization processes are mainly due to the collisions between the excited helium atoms. On the contrary, the He_2^+ density does not change significantly compared to the density plotted from the model.

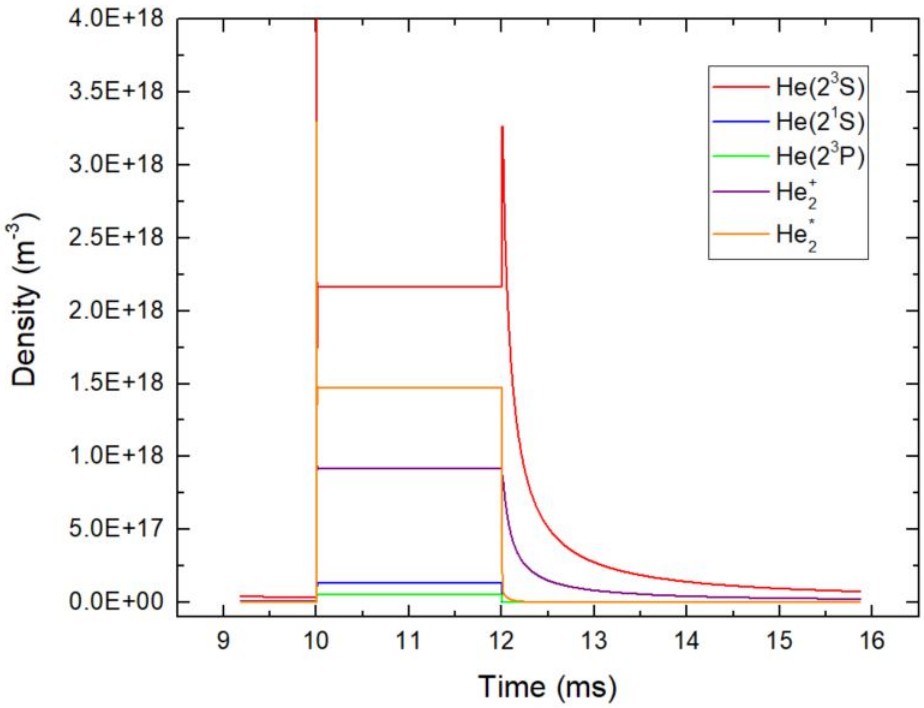

Figure 18: Plot of the densities of different helium species as a function of time. The time span is taken from the second pulse. The electron density equals the He_2^+ density, since He_2^+ is the dominant ion in the plasma and quasineutrality is assumed.

5 Conclusion

The behaviors of the species density and electron temperature over time with the plasma input pulses can be obtained. In this model, they show strong increases and decreases when the power is turned on and off. If the electron temperature reaches a constant value, an equilibrium between the electron production and destruction is observed. This is due to the fact that all rate coefficients will eventually have a constant value, leading to an equilibrium state of the reaction rates. During this steady state, the Penning ionization between two excimers is the dominant production of electrons in the model, while the three-body helium assisted recombination is the main destruction mechanism. A drop of the electron temperature leads to a small increase of the excimer density in a short time. The temperature drop also leads to an increased presence of the Penning ionization reactions, as observed from the electron source plot. This is probably due to the fact that the electrons lose their energy supply, making the heavy particle collision reactions more efficient compared to the electron-involved recombination reactions. The Penning ionization processes create high-energy electrons, which eventually lead to a return of the electron-involved recombination processes. As stated in the theory, Penning ionization is an important process. This is also observed in the simulation.

Several input parameters can be changed in this model. The changed parameters lead to differences in the reaction rates of the chemical reactions, resulting in different plasma behaviors. Conclusions from these changed plasma behaviors are drawn and are given in the following paragraphs.

This model can be applied for different pressure conditions and input powers. The increases of the species densities are not the same with an increasing power. The given pressure of 5 Torr that gives the dominant ion boundary by Deloche et al. [9] is not given with a power input condition. So when looking at the dominant plasma ion, which also can determine the electron density, pressure and power must both be taken into account. An increasing power also means an increasing electron temperature, which for every input power meets a steady state.

A gas temperature change is observed, which changes one order of magnitude during the time the power is turned on. Note that this could only be the case when no power losses to the wall are assumed. Nevertheless, a changing temperature by time should lead to another steady state for the species densities. Namely, changing rate coefficients also lead to a changing equilibrium of the reaction rates. However, the gas temperature is fixed in this model, leading to a discrepancy between the expected rate coefficients and those implemented in the model.

The added reactions are considered to be present in experiments according to the literature. They are elaborated, as well as their corresponding rate coefficients. Some of the reactions that are added to the model are uncertain. Also, some rate coefficients are uncertain or are even unknown. A change of the rate coefficient can lead to a quantity difference of the species. This is shown for the change of the rate coefficient of the process given by equation (59), where the difference was the electron temperature dependence. What could be expected is that a large drop of the electron temperature leads to a higher He_2^+ recombination. However, the change did not lead to a qualitative change of the density decays. This could be due to the stronger induced Penning ionization processes, which respond strongly to the decreased power input, as explained before.

Adding the dissociaton of excimers by atom helium collisions, given by the reverse of equation (43), leads to a substantial decrease of the excimer density. The densities of excited atoms are higher than in the original model. A much stronger decrease of He_2^* is observed when the power is turned off. On the contrary, the density of $He\left(2^3S\right)$ has a certain bump when the power is turned off. This can be due to the heavy particle collisions, which dominates at the moment the power is turned off. On the other hand, the density of He_2^+ does not show a significant change. From this and the previous observation of the changing rate coefficient, it seems like the ratio of the species densities of excited atoms and excimers do not affect the He_2^+ density significantly.

Most models that are developed in the past are tailored to specific plasma conditions. On the contrary, this model provides a more complete set of the possible chemical reactions. The thorough investigation of the possible present chemical reactions provides information for further model de-

velopment of a helium APPJ. Moreover, this model can be used as a basis for further pure helium plasma model developments toward a more complete model that can be used for comparisons with the results from experimental methods. Recommendations for further development of this GPM are given in Section 6. The results and conclusions from the simulations show which behaviors of the plasma can be observed. They therefore show which knowledge eventually can be obtained.

6 Recommendations for further development

Further recommendations in order to improve or upgrade the model are given in this section. Adding more cross sections would lead to a more accurate value of the rate coefficients of the electron-involved reactions. Also, implementing a gas temperature change in time also means a rate coefficient change in time. Diffusion of species can affect the reaction rates due to the change of the species densities. Some of the implemented rate coefficients are uncertain or even unknown. The investigation of these rate coefficients are needed to make the model more accurate. Lastly, radiation trapping should be added. This results in higher densities of certain excited states in the plasma, which eventually lead to higher reaction rates of other chemical reactions. It is necessary to look at higher dimensions of the plasma model when considering diffusion, gas temperature changes and radiation trapping. These phenomena are namely all based on the geometry of the plasma.

6.1 Cross sections

A modified rate coefficient is calculated by detailed balancing in the PLASIMO model for some of the de-excitation reactions according to equation (12). However, the collision cross section σ_{ji} for a superelastic de-excitation from the state j to i could also be calculated by the Klein-Rosseland relation [3]:

$$\sigma_{ji}(\varepsilon) = \frac{g_i}{g_j} \frac{\left(\varepsilon + \varepsilon^*_{ij}\right)}{\varepsilon} \sigma_{ij}\left(\varepsilon + \varepsilon^*_{ij}\right) \tag{90}$$

with ε the electron energy and ε^*_{ij} the energy treshold of the excitation process from i to j [3]. This equation is also deduced from the principle of detailed balancing. Adding the calculated values from equation (90) to the EEDF would result a more accurate representation of the EEDF. This eventually could lead to more accurate rate coefficients of all electron-involved reactions.
Cross sections can determine the shape of the EEDF. Choosing just a rate coefficient of a reaction without the addition of cross sections could eventually result in different rate coefficients of other reactions. A plot of the EEDF could help to show the influences of these cross sections to the EEDF. This plot feature is not present in the PLASIMO software, but can be done with the BOLSIG+ software. It helps to determine whether a rate coefficient can be added with or without the use of cross sections.

6.2 Gas temperature change

The PLASIMO software was not able to calculate the gas temperature change. Therefore, this temperature is assumed constant. This leads to constant rate coefficients if these rate coefficients are only gas temperature dependent. Since the electron temperature is also constant during the power is turned on, this lead to a balance between the reaction and thus the observed steady state. A temperature increase is calculated and presented in Section 4.5. Therefore, it is evident that the gas temperature rate coefficients also change in time. For this reason, it would be expected that a more dynamic change of the electron density is the case. On the other hand, the energy losses due to advection, diffusion or wall losses are not taken into account in this calculation. These processes should be taken into account in order to find a consistent change of the gas temperature.

6.3 Diffusion

Diffusion is neglected in this model. However, this mechanism can lead to a transport of the helium species over time leading to a decrease of the density of species. The reaction rates are dependent on the density of the reactants. As a result, diffusion can affect the reaction rate of certain reactions over time. A diffusion effect is ambipolar diffusion, which is dependent on the electric field. Therefore, the electric field should also be calculated. Some authors neglected reactions because they assumed or stated that the diffusion process is stronger than these reactions. Adding diffusion to the model could therefore give different dominant reactions that take place.

6.4 Reactions and their rate coefficients

Further investigation of some reaction coefficients are needed, since they are not accurately known or based on assumptions. The products from the helium atom assisted recombination of He_2^+ are under debate for example. It is therefore not clear that the added reaction in this model is correct. Moreover, the dominant destruction mechanism of electrons is the helium atom assisted recombination of He_2^+ as mentioned in Section 4.2. However, it is assumed that the He_2^+ is in the lowest rovibrational level. Without this assumption, the rate coefficient of direct recombination will be much higher. Thus, a better look at the decay of the rovibrational states of excimers is needed. Unfortunately, no cross sections for a reaction from higher rovibrational states are present. The excited states with quantum number $n = 3$ or higher are not added to the model. In order to make the model more complete, these excited atoms should also be added. The excitation and de-excitation as well as the ionization of these excited atoms can take part of the stepwize ionization process. Since adding all these excited atoms would make the model quite complicated, an excited state atom with an averaged potential energy could be introduced. The potential energies lie very close to each other as can be seen in Figure 2. The averaged energy comes from the average of all these potential energies of the excited atoms. Using one of possible approaches, cross sections of these (de-)excitations could also be averaged. The cross sections can be found in the work of Ralchenko et al. for example [35]. Carbone et al. [6] made a simple model and compared this model to the experiments of Schregel et al. [39]. They showed that also Rydberg helium molecules and He_3^+ should be added to the model. As mentioned before, the auto-ionization of the Rydberg molecules or doubly excited molecules is a competing process that can increase the efficiency of direct recombination of He_2^+. However, what could be observed is that this process would also happen with the ground state helium assisted recombination of He_2^+, since these Rydberg molecules can be ionized. Emmert et al. [12] stated that the three-body recombination leads to excited atoms. Therefore, there could be a possibility that the three-body recombination has also a same 'path' over the potential line-crossings as for the direct recombination, with also the result of present Rydberg molecules. An investigation of this potential process is recommended.

6.5 Radiation trapping

Radiation trapping is discussed in Section 2.2.4. The derived trapping factor, given by equation (82), is too complex to be implemented in the model when using the PLASIMO software. On the other hand, radiation trapping can be added if only pressure broadening is assumed. The equation can be derived from equations (72) and (76) with a g_0 of 1.6 [21]. An advantage of this method is that a large opacity range can be used. If radiation trapping is added, it will be possible that the excited atom densities change drastically. Namely, the destruction mechanism of $He(2^1P)$ is purely due to radiative decay. Radiation trapping could also be responsible for the reduced decay of the helium molecules with the $A^1\Sigma_u^+$ or $b^3\Pi_g$ energy levels if the transition probabilities are added in the model.

References

[1] L. L. Alves. The IST-LISBON database on LXCat. *Journal of Physics: Conference Series*, 565:012007, dec 2014.

[2] L. L. Alves, G. Gousset, and C. M. Ferreira. A collisional-radiative model for microwave discharges in helium at low and intermediate pressures. *Journal of Physics D: Applied Physics*, 25(12):1713–1732, dec 1992.

[3] T. Belmonte, R. P. Cardoso, G. Henrion, and F. Kosior. Collisional–radiative modelling of a helium microwave plasma in a resonant cavity. 40(23):7343–7356, nov 2007.

[4] H. Bohringer, W. Glebe, and F. Arnold. Temperature dependence of the mobility and association rate coefficient of heions in he from 30-350k. *Journal of Physics B: Atomic and Molecular Physics*, 16(14):2619–2626, jul 1983.

[5] L. Bárdos and H. Baránková. Cold atmospheric plasma: Sources, processes, and applications. *Thin Solid Films*, 518(23):6705 – 6713, 2010.

[6] Emile A. D. Carbone, Christian-Georg Schregel, and Uwe Czarnetzki. Ignition and afterglow dynamics of a high pressure nanosecond pulsed helium micro-discharge: II. rydberg molecules kinetics. *Plasma Sources Science and Technology*, 25(5):054004, sep 2016.

[7] J. Claustre, C. Boukandou-Mombo, J. Margot, J-P. Matte, and F. Vidal. An advanced time-dependent collisional-radiative model of helium plasma discharges. *Plasma Sources Science and Technology*, 26(10):105005, sep 2017.

[8] A J Cunningham, T F O'Malley, and R M Hobson. On the role of vibrational excitation in dissociative recombination. *Journal of Physics B: Atomic and Molecular Physics*, 14(4):773–782, feb 1981.

[9] R. Deloche, P. Monchicourt, M. Cheret, and F. Lambert. High-pressure helium afterglow at room temperature. *Phys. Rev. A*, 13:1140–1176, Mar 1976.

[10] Wolgang Demtröder. *Laser Spectroscopy: basic concepts and instrumentation*. Springer-Verlag Berlin Heidelberg GmbH, 3rd edition, 2003.

[11] Jan Van Dijk, Kim Peerenboom, Manuel Jimenez, Diana Mihailova, and Joost Van Der Mullen. The plasma modelling toolkit plasimo. *Journal of Physics D: Applied Physics*, 42(19):194012, Sep 2009.

[12] F. Emmert, H. H. Angermann, R. Dux, and H. Langhoff. Reaction kinetics of the he(2p) and the he2*(a,v) states in high-density helium. *Journal of Physics D: Applied Physics*, 21(5):667–674, may 1988.

[13] Barbara J. Finlayson-Pitts and James N. Pitts. Chapter 5 - kinetics and atmospheric chemistry. In Barbara J. Finlayson-Pitts and James N. Pitts, editors, *Chemistry of the Upper and Lower Atmosphere*, pages 130 – 178. Academic Press, San Diego, 2000.

[14] Lu Gan, Song Zhang, Devesh Poorun, Dawei Liu, Xinpei Lu, Mengwen He, Xiaoru Duan, and Hongxiang Chen. Medizinische anwendungen von nicht-thermischem atmosphärendruckplasma in der dermatologie. *JDDG: Journal der Deutschen Dermatologischen Gesellschaft*, 16(1):7–14, 2018.

[15] A.F.H. Gessel, van. *Laser diagnostics on atmospheric pressure plasma jets*. PhD thesis, Eindhoven University of Tehchnology Department of Applied Physics, 2013.

[16] Yu. B. Golubovskii, V. A. Maiorov, J. Behnke, and J. F. Behnke. Modelling of the homogeneous barrier discharge in helium at atmospheric pressure. *Journal of Physics D: Applied Physics*, 36(1):39–49, dec 2002.

[17] W.A.A.D. Graef. *Zero-dimensional models for plasma chemistry*. PhD thesis, Eindhoven University of Technology Department of Applied Physics, Jun 2012.

[18] G. J. M. Hagelaar and L. C. Pitchford. Solving the boltzmann equation to obtain electron transport coefficients and rate coefficients for fluid models. *Plasma Sources Science and Technology*, 14(4):722–733, oct 2005.

[19] Peter Collin Hill and Peter Robert Herman. Reaction processes in a $he_2^+(\ ^2\Pi_u \rightarrow a\ ^2\Sigma_g^+)$ flash lamp. *Phys. Rev. A*, 47:4837–4844, Jun 1993.

[20] T. Holstein. Imprisonment of resonance radiation in gases. *Phys. Rev.*, 72:1212–1233, Dec 1947.

[21] T. Holstein. Imprisonment of resonance radiation in gases. ii. *Phys. Rev.*, 83:1159–1168, Sep 1951.

[22] David Huestis. *Radiative Transition Probabilities*, pages 515–533. Springer New York, New York, NY, 2006.

[23] J.F.J. Janssen. *Equilibrium and transport in molecular plasmas*. PhD thesis, Eindhoven University of Technology Department of Applied Physics, Sep 2016.

[24] Jeroen Jonkers, Marco van de Sande, Antonio Sola, Antonio Gamero, Antonio Rodero, and Joost van der Mullen. The role of molecular rare gas ions in plasmas operated at atmospheric pressure. *Plasma Sources Science and Technology*, 12(3):464–474, jul 2003.

[25] A. Köymen, F.-C. Tang, X. Zhao, F.B. Dunning, and G.K. Walters. Multiple activation energies for conversion of $he(2^3s)$ atoms to $he_2(a^3\sigma_u^+)$ molecules in ternary collisions. *Chemical Physics Letters*, 168(5):405 – 409, 1990.

[26] Michael A. Lieberman and Alan J. Lichtenberg. *Principles of Plasma Discharges and Materials Processing*. John Wiley & Sons, 2nd edition, 2005.

[27] J. Liegel, F. Emmert, R. Sauerbrey, and H. Langhoff. Transient absorption of electron beam excited helium in the uv and vuv. *Optics Communications*, 50(2):95 – 100, 1984.

[28] W.C. Martin and W.L. Wiese. Atomic spectroscopy. National Institute of Standards and Technology, URL: https://www.nist.gov/pml/atomic-spectroscopy-compendium-basic-ideas-notation-data-and-formulas, 1999.

[29] J.W. Mills and G.M. Hieftje. A detailed consideration of resonance radiation trapping in the argon inductively coupled plasma. *Spectrochimica Acta Part B: Atomic Spectroscopy*, 39(7):859 – 866, 1984.

[30] G. Myers and A. J. Cunningham. Rate measurements of reactions of helium metastable species at atmospheric pressures. ii. he2 (23+u) in pure afterglows. *The Journal of Chemical Physics*, 67(5):1942–1947, 1977.

[31] Gary Myers and A. J. Cunningham. Rate measurements of reactions of helium metastable species at atmospheric pressures. i. he (23s) in pure afterglows. *The Journal of Chemical Physics*, 67(1):247–253, 1977.

[32] H. B. Pedersen, H. Buhr, S. Altevogt, V. Andrianarijaona, H. Kreckel, L. Lammich, N. de Ruette, E. M. Staicu-Casagrande, D. Schwalm, D. Strasser, X. Urbain, D. Zajfman, and A. Wolf. Dissociative recombination and low-energy inelastic electron collisions of the helium dimer ion. *Phys. Rev. A*, 72:012712, Jul 2005.

[33] A. V. Phelps and J. P. Molnar. Lifetimes of metastable states of noble gases. *Phys. Rev.*, 89:1202–1208, Mar 1953.

[34] Leanne C. Pitchford, Luis L. Alves, Klaus Bartschat, Stephen F. Biagi, Marie-Claude Bordage, Igor Bray, Chris E. Brion, Michael J. Brunger, Laurence Campbell, Alise Chachereau, Bhaskar Chaudhury, Loucas G. Christophorou, Emile Carbone, Nikolay A. Dyatko, Christian M. Franck, Dmitry V. Fursa, Reetesh K. Gangwar, Vasco Guerra, Pascal Haefliger, Gerjan J. M. Hagelaar, Andreas Hoesl, Yukikazu Itikawa, Igor V. Kochetov, Robert P. McEachran, W. Lowell Morgan, Anatoly P. Napartovich, Vincent Puech, Mohamed Rabie, Lalita Sharma, Rajesh Srivastava, Allan D. Stauffer, Jonathan Tennyson, Jaime de Urquijo, Jan van Dijk, Larry A. Viehland, Mark C. Zammit, Oleg Zatsarinny, and Sergey Pancheshnyi. Lxcat: an open-access, web-based platform for data needed for modeling low temperature plasmas. *Plasma Processes and Polymers*, 14(1-2):1600098, 2017.

[35] Yu. Ralchenko, R.K. Janev, T. Kato, D.V. Fursa, I. Bray, and F.J. de Heer. Electron-impact excitation and ionization cross sections for ground state and excited helium atoms. *Atomic Data and Nuclear Data Tables*, 94(4):603 – 622, 2008.

[36] Shahid Rauf and Mark J. Kushner. Dynamics of a coplanar-electrode plasma display panel cell. i. basic operation. *Journal of Applied Physics*, 85(7):3460–3469, 1999.

[37] J. E. Russell. Analysis of the reaction he++he+he→he+2+he. ii. improved sampling. *The Journal of Chemical Physics*, 84(8):4394–4400, 1986.

[38] M. Santos, C. Noël, T. Belmonte, and L. L. Alves. Microwave capillary plasmas in helium at atmospheric pressure. *Journal of Physics D: Applied Physics*, 47(26):265201, jun 2014.

[39] Christian-Georg Schregel, Emile A. D. Carbone, Dirk Luggenhölscher, and Uwe Czarnetzki. Ignition and afterglow dynamics of a high pressure nanosecond pulsed helium micro-discharge: I. electron, rydberg molecules and he (23s) densities. *Plasma Sources Science and Technology*, 25(5):054003, sep 2016.

[40] A. Schütze, J. Y. Jeong, S. E. Babayan, Jaeyoung Park, G. S. Selwyn, and R. F. Hicks. The atmospheric-pressure plasma jet: a review and comparison to other plasma sources. *IEEE Transactions on Plasma Science*, 26(6):1685–1694, Dec 1998.

[41] G.S. Selwyn, H.W. Herrmann, J. Park, and I. Henins. Materials processing using an atmospheric pressure, rf-generated plasma source. *Contributions to Plasma Physics*, 41(6):610–619, 2001.

[42] Boris M. Smirnov. *Theory of gas discharge plasma*. Springer International Publishing Switzerland, 2015.

[43] J. Stevefelt, J. M. Pouvesle, and A. Bouchoule. Reaction kinetics of a high pressure helium fast discharge afterglow. *The Journal of Chemical Physics*, 76(8):4006–4015, 1982.

[44] Marc van der Schans, Bart Platier, Peter Koelman, Ferdi van de Wetering, Jan van Dijk, Job Beckers, Sander Nijdam, and Wilbert IJzerman. Decay of the electron density and the electron collision frequency between successive discharges of a pulsed plasma jet in n2. *Plasma Sources Science and Technology*, 28(3):035020, mar 2019.

[45] Roger J. van Sonsbeek, Ronald Cooper, and R. N. Bhave. Pulse radiolysis studies of ion–electron recombination in helium. pressure and temperature effects. *The Journal of Chemical Physics*, 97(3):1800–1808, 1992.

[46] P. J. Walsh. Effect of simultaneous doppler and collision broadening and of hyperfine structure on the imprisonment of resonance radiation. *Phys. Rev.*, 116:511–515, Nov 1959.

[47] Qiang Wang, Demetre J. Economou, and Vincent M. Donnelly. Simulation of a direct current microplasma discharge in helium at atmospheric pressure. *Journal of Applied Physics*, 100(2):023301, 2006.

[48] W. L. Wiese and J. R. Fuhr. Accurate atomic transition probabilities for hydrogen, helium, and lithium. *Journal of Physical and Chemical Reference Data*, 38(3):565–720, 2009.

[49] J Winter, R Brandenburg, and K-D Weltmann. Atmospheric pressure plasma jets: an overview of devices and new directions. *Plasma Sources Science and Technology*, 24(6):064001, oct 2015.

[50] Xiaohui Yuan and L. L. Raja. Computational study of capacitively coupled high-pressure glow discharges in helium. *IEEE Transactions on Plasma Science*, 31(4):495–503, Aug 2003.

[51] X. Zhao, P. A. Soletsky, W. H. Bryan, F. B. Dunning, and G. K. Walters. Temperature dependence of he(2 $^3\mathrm{p}_j$) reactions: Collision-induced mixing and conversion to $\mathrm{he}_2(\ ^3\Pi_\mathrm{g})$ molecules. *Phys. Rev. A*, 48:4350–4357, Dec 1993.

A Input file

The code for the global model made in PLASIMO can be found at `https://epgmod.phys.tue.nl/gitlab/plasimo/Bachelor/thomasvandenbiggelaar.git`. Access can be requested by contacting dr. D.B. Mihailova, diana@plasma-matters.nl. Version of the used PLASIMO software is Version 6.1, Developer's version Windows 64 Bit, downloaded on April 30th 2019.
The initial plasma densities of the excited and ionized species are chosen arbitrarily. However, it should be noted that these values are in a certain range. This is because of the fact that the solver, which calculates the output values by iteration, must converge. The software does not take the weights of the species into account. However, if equations like equation (79) are implemented in the model, these weights must be taken into account. Namely, the software has an option to use the input weight values of the species into equations, which are called declarations in the software. Also, a careful look at the stepper is recommended. This is the time width between two calculations. If the stepper is too large, this leads to bad output values. However, a too small stepper results in large calculation times.